NASA Technical Memorandum 4548

Predicting the Effects of Unmodeled Dynamics on an Aircraft Flight Control System Design Using Eigenspace Assignment

Eric N. Johnson, John B. Davidson, and Patrick C. Murphy

June 1994

NASA Technical Memorandum 4548

Predicting the Effects of Unmodeled Dynamics on an Aircraft Flight Control System Design Using Eigenspace Assignment

Eric N. Johnson
The George Washington University • Washington, D.C.

John B. Davidson and Patrick C. Murphy
Langley Research Center • Hampton, Virginia

National Aeronautics and Space Administration
Langley Research Center • Hampton, Virginia 23681-0001

June 1994

Abstract

When using eigenspace assignment to design an aircraft flight control system, one must first develop a model of the plant. Certain questions arise when creating this model as to which dynamics of the plant need to be included in the model and which dynamics can be left out or approximated. The answers to these questions are important because a poor choice can lead to closed-loop dynamics that are unpredicted by the design model. To alleviate this problem, a method has been developed for predicting the effect of not including certain dynamics in the design model on the final closed-loop eigenspace. This development provides insight as to which characteristics of unmodeled dynamics will ultimately affect the closed-loop rigid-body dynamics. What results from this insight is a guide for eigenstructure control law designers to aid them in determining which dynamics need or do not need to be included and a new way to include these dynamics in the flight control system design model to achieve a required accuracy in the closed-loop rigid-body dynamics. The method is illustrated for a lateral-directional flight control system design using eigenspace assignment for the NASA High Alpha Research Vehicle (HARV).

Introduction

Fidelity of the design model is a chief concern in any control law design process. In this context, fidelity of the design model corresponds to how well a control law, which is designed using this model, achieves design objectives when applied to the actual system. A fidelity issue was raised in the design of a research lateral-directional control law (ref. 1) for NASA's F/A-18 High Alpha Research Vehicle (HARV). The control law was synthesized with the CRAFT (control power, robustness, agility, and flying-qualities trade-offs) design methodology (ref. 2), which is a graphical method that uses eigenspace placement methods (refs. 3 and 4). Only rigid-body dynamics were considered; other dynamics, such as actuators, were neglected. It was noted, however, that when the other dynamics were included, the closed-loop rigid-pole locations varied from those predicted by the low-order design model. In this report, a method is developed to determine which dynamics need to be included in a control law synthesis procedure that uses eigenspace assignment.

Elements of the aircraft rigid-body eigenspace are well understood, and much is known about desirable dynamic characteristics (ref. 5). However, the aircraft has dynamics besides those of the rigid body (e.g., actuators, control system filters, and transport delays). Exactly which dynamics will significantly affect the design is normally not known at the outset of the control law design process.

A controller can be synthesized using a system with dynamics beyond those of the rigid body, but this occurs at a cost. First, the relationship between the desired eigenspace and the dynamics of the closed-loop aircraft becomes less obvious. Second, the speed at which a given set of feedback gains can be generated for an iteration of the desired eigenspace is reduced. This reduction results in a trade-off between the simplicity and speed of a flight control system design iteration and the accuracy of the final design. The fundamental question is: what error will result if certain dynamics are neglected? The answer to this question will provide insight into the relationship between given unmodeled dynamics and their effect on the rigid-body dynamics of the full-order, closed-loop system.

To provide a clear exposition of the key results, the report is organized as follows. The HARV control law design is presented in detail as the motivator of this research. The rigid-body system used to synthesize the controller and the unmodeled higher order dynamics are described. Next, a single-input, single-output (SISO) example of the effect of unmodeled dynamics is presented. This example provides the conceptual basis for the multiple-input, multiple-output (MIMO) work presented.

Symbols

$\mathbf{A}$	stability matrix
$\mathbf{B}$	control matrix

$\mathbf{E}$	eigenspace transformation matrix
e	number of effectors
$\mathbf{G}$	feedback gain matrix
g	gravitational acceleration, g units, $1g = 32.2$ ft/sec^2
$\mathbf{I}$	identity matrix
$\mathbf{K}$	feed-forward gain matrix
k	reduction factor
k_{FB}	feedback gain
$L_{v,p,r,\delta_{()}}$	roll moment dimensional stability and control derivatives
l	number of measurements
$\mathbf{M}$	measurement matrix
m	number of controls
$\mathbf{N}$	feed-through matrix
$N_{v,p,r,\delta_{()}}$	yaw moment dimensional stability and control derivatives
n	number of states of low-order system
n_y	lateral acceleration, g units
p	roll angular rate, rad/sec
$\mathbf{Q}$	feed-through term effect on augmentation matrix
$\underline{R}$	real number set
r	yaw angular rate, rad/sec
s	Laplace transform variable
$\mathbf{T}$	time constant matrix
$TF(s)$	transfer function
t_d	transport delay time, sec
$\mathbf{u}$	control vector
$\mathbf{V}$	eigenvector matrix
V_T	airspeed, ft/sec
$\mathbf{v}$	higher order states
v_s	lateral velocity, ft/sec
$\mathbf{w}$	unmodeled filter output
$\mathbf{x}$	state vector of rigid-body system
$Y_{v,p,\delta_{()}}$	side force dimensional stability and control derivatives
$\mathbf{z}$	measurement vector used for feedback
α	angle of attack, deg
β	sideslip angle, rad
γ	flight path angle, rad
δ	control effector deflection angle, deg
ζ	damping ratio
$\mathbf{\Lambda}$	eigenvalue matrix
λ	eigenvalue or pole
$\boldsymbol{\nu}$	eigenvector
τ	time constant
ϕ_s	bank angle, deg
ω	natural frequency, rad/sec

Subscripts:

ail	aileron
as	asymmetric stabilator
b	body-axis measurement
c	commanded
comp	computed
den	denominator
e	associated with lag in effectors
F	unmodeled filters in parallel
f	unmodeled filter
FB	feedback
FO	full-order, closed-loop system
HO	unmodeled, higher order dynamics
i	index
l	associated with lag in measurement
LO	low-order, closed-loop system
m	associated with lag in control
num	numerator
pilot	pilot commanded
rb	rigid-body pole
$()_{rb}$	rigid-body dynamics of ( )
RO	roll-off filter
rtv	roll thrust vectoring
rud	rudder
s	state
sens	sensed value
slow	increased time constant matrix
ytv	yaw thrust vectoring

Superscripts:

T	transpose
.	time derivative
$\hat{}$	predicted
*	conjugate transpose

Abbreviations:

CRAFT	control power, robustness, agility, and flying-qualities trade-offs
DEA	direct eigenspace assignment
HARV	High Alpha Research Vehicle
HATP	High-Angle-of-Attack Technology Program
MIMO	multiple-input/multiple-output
SISO	single-input/single-output

Background

HARV Description

The analysis presented is motivated by a research lateral-directional flight control system design for the High Alpha Research Vehicle (HARV), which is shown in figure 1. The HARV is part of the NASA High-Angle-of-Attack Technology Program (HATP), and it will provide flight validation of HATP research and technology. The HARV is a preproduction F/A-18 that has been modified with a thrust vectoring system, as shown in figure 2. The thrust vectoring is designed to provide additional control moments for high angle-of-attack flight. The HARV has a research flight control system designed to simplify the installation and the modification of control laws. One intent is to provide flight validation of experimental high angle-of-attack control systems.

Low-Order Aircraft Model

The research lateral-directional flight control system is designed using linear models of the aircraft at various flight conditions. For these models, the rigid-body dynamics are fourth order. The states include lateral velocity, roll rate, yaw rate, and bank angle. The control effectors are aileron, rudder, asymmetric stabilator, yaw thrust vectoring, and roll thrust vectoring. The measurements are roll rate, yaw rate, lateral acceleration, and computed sideslip rate. The lateral acceleration sensor is located near the pilot station, thus preventing the similarity with sensed sideslip rate that would occur if it were at the aircraft center of gravity.

The low-order, open-loop aircraft model can be written as

$$\dot{\mathbf{x}} = \mathbf{A}\mathbf{x} + \mathbf{B}\mathbf{u}$$

$$\mathbf{z} = \mathbf{M}\mathbf{x} + \mathbf{N}\mathbf{u}$$

The state, measurement, and control effector vectors are

$$\mathbf{x}^T = (v_s, p_s, r_s, \phi_s)$$

$$\mathbf{z}^T = (p_b, r_b, n_{y_{\text{sens}}}, \dot{\beta}_{\text{comp}})$$

$$\mathbf{u}^T = (\delta_{\text{ail}}, \delta_{\text{rud}}, \delta_{as}, \delta_{\text{ytv}}, \delta_{\text{rtv}})$$

The measurement equation $\mathbf{z}$ is defined by $\mathbf{M}$ and $\mathbf{N}$ matrices to distinguish it from the traditional output equation. These measurements are assumed to have no noise. The elements of stability, control, measurement, and feed-through matrices, at a single flight condition, are defined as

$$\mathbf{A} = \begin{bmatrix} Y_v & Y_p & -V_T & g\cos\gamma \\ L_v & L_p & L_r & 0 \\ N_v & N_p & N_r & 0 \\ 0 & 1 & \tan\gamma & 0 \end{bmatrix}$$

$$\mathbf{B} = \begin{bmatrix} Y_{\delta_{\text{ail}}} & Y_{\delta_{\text{rud}}} & Y_{\delta_{as}} & Y_{\delta_{\text{ytv}}} & Y_{\delta_{\text{rtv}}} \\ L_{\delta_{\text{ail}}} & L_{\delta_{\text{rud}}} & L_{\delta_{as}} & L_{\delta_{\text{ytv}}} & L_{\delta_{\text{rtv}}} \\ N_{\delta_{\text{ail}}} & N_{\delta_{\text{rud}}} & N_{\delta_{as}} & N_{\delta_{\text{ytv}}} & N_{\delta_{\text{rtv}}} \\ 0 & 0 & 0 & 0 & 0 \end{bmatrix}$$

$$\mathbf{M} = \begin{bmatrix} 0 & \cos\alpha & -\sin\alpha & 0 \\ 0 & \sin\alpha & \cos\alpha & 0 \\ n_{y_v} & n_{y_p} & n_{y_r} & 0 \\ \dot{\beta}_v & \dot{\beta}_p & \dot{\beta}_r & \dot{\beta}_\phi \end{bmatrix}$$

$$\mathbf{N} = \begin{bmatrix} 0 & 0 & 0 & 0 & 0 \\ 0 & 0 & 0 & 0 & 0 \\ n_{y_{\delta_{\text{ail}}}} & n_{y_{\delta_{\text{rud}}}} & n_{y_{\delta_{as}}} & n_{y_{\delta_{\text{ytv}}}} & n_{y_{\delta_{\text{rtv}}}} \\ \dot{\beta}_{\delta_{\text{ail}}} & \dot{\beta}_{\delta_{\text{rud}}} & \dot{\beta}_{\delta_{as}} & \dot{\beta}_{\delta_{\text{ytv}}} & \dot{\beta}_{\delta_{\text{rtv}}} \end{bmatrix}$$

Flight conditions range from angles of attack of 2.5° to 60° at a constant altitude of 25 000 ft in unaccelerated flight.

For this HARV control law design, the states chosen above lead to classically defined spiral, roll, and Dutch roll modes (at low angle of attack). The models used for all examples presented in this work are listed in appendix A.

Low-Order, Closed-Loop System

The components of the flight control system corresponding to the low-order, closed-loop system, shown in figure 3, consist of feed-forward and feedback

L-91-09766

Figure 1. High Alpha Research Vehicle (HARV).

L-91-14327

Figure 2. HARV thrust-vectoring system.

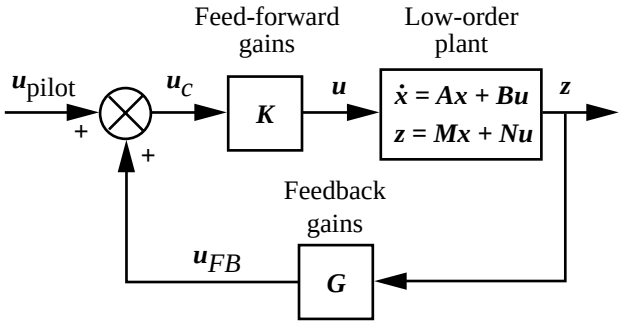

Figure 3. Low-order, closed-loop system.

gains. The feed-forward gain matrix maps two inputs into the five aircraft control effectors. These two inputs are commanded roll and yaw angular accelerations such that

$$\mathbf{u}_c^T = (\dot{p}_c, \dot{r}_c)$$

The feed-forward gain matrix is a Jacobian of a control mapping algorithm, which is discussed in reference 6. For the purposes of the research presented, it is assumed that the feed-forward gain matrix is given. The feedback gains will be used to place closed-loop dynamics. Here, the commanded angular acceleration is referred to as the controls, and the five inputs to the aircraft are called effectors. The controls then become the sum of pilot input and feedback. The feedback gain matrix maps the four measurements into these two controls.

The control system synthesis technique used to generate the lateral-directional flight control system was the CRAFT approach based on the direct eigenspace assignment (DEA) of references 2, 3, and 4. The CRAFT process provides a graphical approach to trade agility, robustness, flying qualities, and control power. This approach utilizes DEA to achieve the desired dynamics selected using the CRAFT technique. The DEA generates linear measurement feedback gains as a function of the design model and a desired closed-loop eigenspace. Here, the design model contains only the rigid-body aircraft dynamics. The design model and control law can be expressed as

$$\dot{\mathbf{x}} = \mathbf{A}\mathbf{x} + \mathbf{B}\mathbf{u} \qquad \text{(System dynamics)} \quad (1)$$

$$\mathbf{z} = \mathbf{M}\mathbf{x} + \mathbf{N}\mathbf{u} \qquad \text{(System measurements)} \quad (2)$$

$$\mathbf{u} = \mathbf{K}\mathbf{u}_c \qquad \text{(Feed-forward control)} \quad (3)$$

$$\mathbf{u}_c = \mathbf{u}_{FB} + \mathbf{u}_{\text{pilot}} \qquad \text{(Feed-forward control)} \quad (4)$$

$$\mathbf{u}_{FB} = \mathbf{G}\mathbf{z} \qquad \text{(Feedback control)} \quad (5)$$

with n states, m controls, l measurements, and e effectors, thus making $\mathbf{x} \in \underline{R}^n$, $\mathbf{u}_c \in \underline{R}^m$, $\mathbf{z} \in \underline{R}^l$, and $\mathbf{u} \in \underline{R}^e$. To derive an expression for the closed-loop system, equations (4) and (5) can be substituted into equation (3) to get

$$\mathbf{u} = \mathbf{K}\mathbf{G}\mathbf{z} + \mathbf{K}\mathbf{u}_{\text{pilot}}$$

Equation (2) is then used for $\mathbf{z}$ such that

$$\mathbf{u} = \mathbf{K}\mathbf{G}\mathbf{M}\mathbf{x} + \mathbf{K}\mathbf{G}\mathbf{N}\mathbf{u} + \mathbf{K}\mathbf{u}_{\text{pilot}}$$

Solving for $\mathbf{u}$,

$$\mathbf{u} = (\mathbf{I} - \mathbf{K}\mathbf{G}\mathbf{N})^{-1}\mathbf{K}\mathbf{G}\mathbf{M}\mathbf{x} + (\mathbf{I} - \mathbf{K}\mathbf{G}\mathbf{N})^{-1}\mathbf{K}\mathbf{u}_{\text{pilot}}$$

By using this equation for $\mathbf{u}$ in equation (1), the closed-loop system can be stated as

$$\dot{\mathbf{x}} = [\mathbf{A} + \mathbf{B}(\mathbf{I} - \mathbf{K}\mathbf{G}\mathbf{N})^{-1}\mathbf{K}\mathbf{G}\mathbf{M}]\mathbf{x} + \mathbf{B}(\mathbf{I} - \mathbf{K}\mathbf{G}\mathbf{N})^{-1}\mathbf{K}\mathbf{u}_{\text{pilot}}$$

or in shorthand as

$$\dot{\mathbf{x}} = \mathbf{A}_{LO}\mathbf{x} + \mathbf{B}_{LO}\mathbf{u}_{\text{pilot}}$$

As previously discussed, the feed-forward gains define the effector blending used, and the feedback gains are synthesized to achieve a desired closed-loop eigenspace. For the system described, the feedback gain matrix will place l eigenvalues. The DEA will also exactly place m elements of the l corresponding eigenvectors, or alternatively, it will achieve a least-squares fit of i elements of an individual eigenvector, where $m < i \leq n$.

For the purposes of feedback gain synthesis, there are four states, four measurements, five effectors, and two controls. This implies exact placement of the poles for the low-order, closed-loop system. Also, two eigenvector elements can be exactly placed for each mode. The feedback gains are designed to be scheduled with angle of attack. The feed-forward gains are scheduled primarily with angle of attack, dynamic pressure, and thrust. Appendix B contains baseline feed-forward and feedback gain matrices.

Full-Order, Closed-Loop System

The complete aircraft plus control system has dynamics beyond that of the system previously described. This includes other aircraft dynamics, such as actuator dynamics, and additional elements of the control system, such as structural notch filters. The layout of this control system and plant model is shown in figure 4.

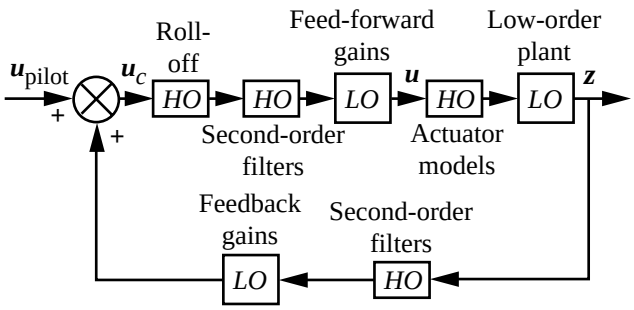

Figure 4. Layout of HARV lateral-directional control system and plant model which differentiates low-order and higher order, unmodeled dynamics.

Models of the actuator dynamics are available in reference 7. These actuator models range from first order to eighth order for each of the five actuators.

Various flight control system filters are also not included in the design process. These include first-order, roll-off filters of 25 rad/sec, which are placed on each of the controls as part of the flight control system design. A notch filter is also placed on each of the controls as well as on each of the measurements. An exception is the sensed lateral acceleration channel that has two notch filters in series.

Here, the HARV full-order, closed-loop system will have 25 states. In the following development, however, not all unmodeled dynamics will be initially considered. The term full-order, closed-loop system will be used to describe a closed-loop system consisting of the open-loop, rigid-body dynamics, the feed-forward and feedback gains, and the particular unmodeled dynamics under consideration.

Spectral Decomposition

To evaluate full-order, closed-loop system dynamics, consider the portion of the eigenspace that corresponds to the rigid-body system. When the unmodeled dynamics are of sufficiently higher frequency than the low-order, closed-loop system, or they are outside the bandwidth of the pilot, the dynamics that are dominant to the pilot will be determined by the rigid-body eigenspace. The rigid-body eigenspace is a combination of the rigid-body eigenvalues and eigenvector elements that are associated with the rigid-body modes. As an example, the rigid-body roll pole of the low-order, closed-loop system and of the 25-state system is shown in figure 5 as a function of angle of attack.

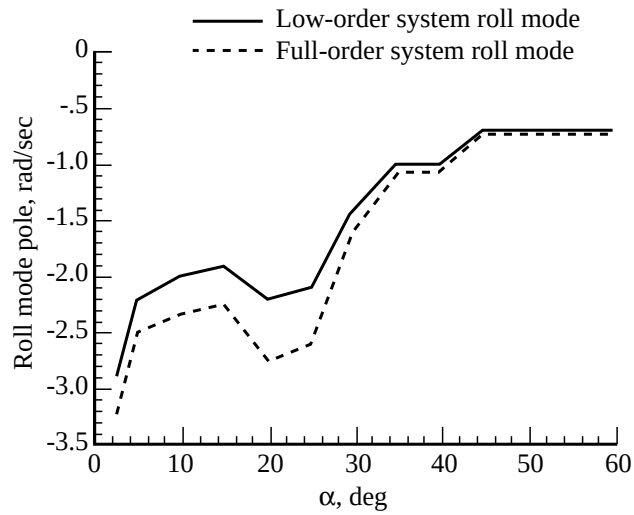

Figure 5. Low-order system and full-order, closed-loop system roll pole.

The full-order, closed-loop system has dynamics defined by

$$\dot{\mathbf{x}} = \mathbf{A}_{FO}\mathbf{x} + \mathbf{B}_{FO}\mathbf{u}_{\text{pilot}}$$

The rigid-body eigenspace is characterized here by a spectral decomposition of $\mathbf{A}_{FO}$ such that

$$\mathbf{A}_{FO}\mathbf{V} = \mathbf{V}\boldsymbol{\Lambda}$$

The eigenvalue and eigenvector matrices are then partitioned to separate the eigenspace of interest so that

$$\mathbf{V} = \begin{bmatrix} \mathbf{V}_{11} & \mathbf{V}_{12} \\ \mathbf{V}_{21} & \mathbf{V}_{22} \end{bmatrix}$$

$$\boldsymbol{\Lambda} = \begin{bmatrix} \boldsymbol{\Lambda}_1 & 0 \\ 0 & \boldsymbol{\Lambda}_2 \end{bmatrix}$$

where $\boldsymbol{\Lambda}_1$ is a square matrix containing achieved rigid-body eigenvalues on its diagonal and $\mathbf{V}_{11}$ is a square matrix containing achieved rigid-body eigenvector elements associated with rigid-body states. Ideally, one would like to compare the eigenspace of the low-order, closed-loop system with the eigenspace of

$$(\mathbf{A}_{FO})_{rb} \equiv \mathbf{V}_{11}\boldsymbol{\Lambda}_1\mathbf{V}_{11}^{-1}$$

(i.e., the rigid-body eigenspace of the full-order, closed-loop system). This matrix has the same dimensions as the low-order, closed-loop system matrix $\mathbf{A}_{LO}$.

Although this reduced-order system is not a substitute for a look at frequency response and time histories of the full-order system, it does allow the control law designer to compare the dynamics of the full-order, closed-loop system with well-understood aircraft rigid-body dynamics. Also, knowledge of the achieved rigid-body eigenspace is important because its relationship with the desired dynamics fundamentally determines whether or not certain dynamics can be omitted from the design model.

Eigenspace Transformation Matrix

A concept that will appear repeatedly in this work is that of a single matrix transformation in the form

$$\mathbf{A}_{LO} = \mathbf{E}(\mathbf{A}_{FO})_{rb}$$

where $\mathbf{A}_{LO}$ is the low-order, closed-loop system matrix and $(\mathbf{A}_{FO})_{rb}$ is composed of the rigid-body portion of the full-order, closed-loop system eigenspace, as described in the section entitled "Spectral Decomposition." The term $\mathbf{E}$ will be referred to as an eigenspace transformation matrix. Although $\mathbf{A}_{LO}$ and $(\mathbf{A}_{FO})_{rb}$ are not actually the eigenspaces, their eigenvalues and eigenvectors are the rigid-body eigenspace of the low- and full-order closed-loop systems, respectively. All three of these matrices are square, and they have dimensions equal to the number of states in the rigid-body system. As the unmodeled dynamics become less significant to the achieved rigid-body eigenspace, the eigenspace transformation matrix should approach the identity matrix.

A look at the most significant contributors to the eigenspace transformation matrix may provide insight into what causes the rigid-body dynamics to differ from those of the low-order, closed-loop system. If the effect on the rigid-body eigenspace can be easily calculated, such a calculation could be useful in determining whether certain dynamics can be left out of the design model.

SISO Example

To facilitate the discussion of the multiple-input/multiple-output (MIMO) results in this report, a single-input/single-output (SISO) example is now presented. The SISO system (fig. 6) presented is a first-order roll mode approximation of the HARV at an angle of attack of 5°. Aileron deflection is the plant input, and roll rate is the plant output. The first-order lag aileron actuator model is the unmodeled dynamics in this example.

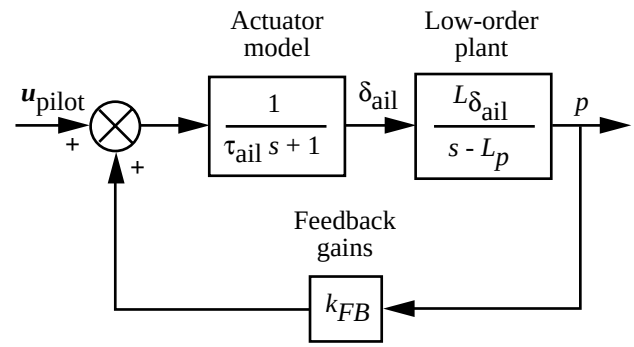

Figure 6. SISO example with first-order roll mode approximation at angle of attack of 5°.

For the purposes of control law design, the first-order lag aileron actuator is not included in the design model. This SISO low-order, closed-loop design model can be written as

$$\frac{p(s)}{u_{\text{pilot}}(s)} = \frac{L_{\delta_{\text{ail}}}}{s - L_p - L_{\delta_{\text{ail}}} k_{FB}} \tag{6}$$

With the actuator model, this full-order, closed-loop system has two states, and it can be written as

$$\frac{p(s)}{u_{\text{pilot}}(s)} = \frac{L_{\delta_{\text{ail}}}}{(\tau_{\text{ail}} s + 1)(s - L_p) - L_{\delta_{\text{ail}}} k_{FB}} \tag{7}$$

In state space, this full-order, closed-loop system is expressed as

$$\begin{Bmatrix} \dot{p} \\ \dot{\delta}_{\text{ail}} \end{Bmatrix} = \begin{bmatrix} L_p & L_{\delta_{\text{ail}}} \\ \tau_{\text{ail}}^{-1} k_{FB} & -\tau_{\text{ail}}^{-1} \end{bmatrix} \begin{Bmatrix} p \\ \delta_{\text{ail}} \end{Bmatrix} + \begin{Bmatrix} 0 \\ \tau_{\text{ail}}^{-1} \end{Bmatrix} u_{\text{pilot}}$$

The low-order, closed-loop system has one state, with the eigenvalue

$$\lambda_{LO} = L_p + L_{\delta_{\text{ail}}} k_{FB} \tag{8}$$

which is the desired roll mode pole. The full-order, closed-loop stability matrix is

$$\mathbf{A}_{FO} = \begin{bmatrix} L_p & L_{\delta_{\text{ail}}} \\ \tau_{\text{ail}}^{-1} k_{FB} & -\tau_{\text{ail}}^{-1} \end{bmatrix}$$

Of interest are the eigenvalues and eigenvectors of this closed-loop system corresponding to the rigid-body dynamics, or roll mode. The eigenvalue is $\lambda_{FO_{rb}}$ and the eigenvector is $\boldsymbol{\nu}_{11}$ when this full-order, closed-loop system matrix is written as the spectral decomposition

$$\begin{bmatrix} L_p & L_{\delta_{\text{ail}}} \\ \tau_{\text{ail}}^{-1} k_{FB} & -\tau_{\text{ail}}^{-1} \end{bmatrix} \begin{bmatrix} \nu_{11} & \nu_{12} \\ \nu_{21} & \nu_{22} \end{bmatrix} = \begin{bmatrix} \nu_{11} & \nu_{12} \\ \nu_{21} & \nu_{22} \end{bmatrix} \begin{bmatrix} \lambda_{FO_{rb}} & 0 \\ 0 & \lambda_{HO} \end{bmatrix}$$

Note that $\lambda_{FO_{rb}}$ and ν_{11} are scalars and that, in the absence of ν_{21}, ν_{11} is arbitrary. In this development, only the upper left and lower left partitions of the above matrix equation are needed such that

$$L_p\nu_{11} + L_{\delta_{\text{ail}}}\nu_{21} = \nu_{11}\lambda_{FO_{rb}} \tag{9}$$

$$\tau_{\text{ail}}^{-1}k_{FB}\nu_{11} - \tau_{\text{ail}}^{-1}\nu_{21} = \nu_{21}\lambda_{FO_{rb}} \tag{10}$$

Now, the goal is to eliminate ν_{21} and solve for λ_{LO} in terms of $\lambda_{FO_{rb}}$. The method that proves successful when working with the MIMO system is the following. Equations (9) and (10) are rewritten as

$$L_p\nu_{11} - \nu_{11}\lambda_{FO_{rb}} = -L_{\delta_{\text{ail}}}\nu_{21} \tag{11}$$

$$k_{FB}\nu_{11} = \nu_{21} + \tau_{\text{ail}}\nu_{21}\lambda_{FO_{rb}} \tag{12}$$

Equation (11) is expanded into an infinite series such that each term contains the right-hand side of equation (12). To start this expansion into an infinite series, add and subtract $-L_p\tau_{\text{ail}}\nu_{21}\lambda_{FO_{rb}}$ and group terms to give

$$\begin{aligned} L_p\nu_{11} - \nu_{11}\lambda_{FO_{rb}} = &- L_{\delta_{\text{ail}}}(\nu_{21} + \tau_{\text{ail}}\nu_{21}\lambda_{FO_{rb}}) \\ &+ L_{\delta_{\text{ail}}}\tau_{\text{ail}}\nu_{21}\lambda_{FO_{rb}} \end{aligned}$$

Continuing in a similar manner by adding and subtracting

$$(-1)^i L_{\delta_{\text{ail}}}\tau_{\text{ail}}^i\nu_{21}\lambda_{FO_{rb}}^i \qquad (i = 2, 3, \ldots, \infty)$$

and grouping terms to get the right-hand side of equation (12) in each term yields the infinite series

$$\begin{aligned} L_p\nu_{11} - \nu_{11}\lambda_{FO_{rb}} = &-L_{\delta_{\text{ail}}}(\nu_{21} + \tau_{\text{ail}}\nu_{21}\lambda_{FO_{rb}}) \\ &+ L_{\delta_{\text{ail}}}\tau_{\text{ail}}(\nu_{21} + \tau_{\text{ail}}\nu_{21}\lambda_{FO_{rb}})\lambda_{FO_{rb}} \\ &- L_{\delta_{\text{ail}}}\tau_{\text{ail}}^2(\nu_{21} + \tau_{\text{ail}}\nu_{21}\lambda_{FO_{rb}})\lambda_{FO_{rb}}^2 \\ &+ L_{\delta_{\text{ail}}}\tau_{\text{ail}}^3(\nu_{21} + \tau_{\text{ail}}\nu_{21}\lambda_{FO_{rb}})\lambda_{FO_{rb}}^3 \cdots \end{aligned}$$

Then eliminate ν_{21} by using equation (12) so that

$$\begin{aligned} L_p\nu_{11} - \nu_{11}\lambda_{FO_{rb}} = &-L_{\delta_{\text{ail}}}k_{FB}\nu_{11} + L_{\delta_{\text{ail}}}\tau_{\text{ail}}k_{FB}\lambda_{FO_{rb}}\nu_{11} \\ &- L_{\delta_{\text{ail}}}\tau_{\text{ail}}^2k_{FB}\lambda_{FO_{rb}}^2\nu_{11} \\ &+ L_{\delta_{\text{ail}}}\tau_{\text{ail}}^3k_{FB}\lambda_{FO_{rb}}^3\nu_{11} \cdots \end{aligned}$$

Dividing out the now arbitrary ν_{11}, the above becomes

$$\begin{aligned} L_p - \lambda_{FO_{rb}} = &-L_{\delta_{\text{ail}}}k_{FB} + L_{\delta_{\text{ail}}}\tau_{\text{ail}}k_{FB}\lambda_{FO_{rb}} \\ &- L_{\delta_{\text{ail}}}\tau_{\text{ail}}^2k_{FB}\lambda_{FO_{rb}}^2 + L_{\delta_{\text{ail}}}\tau_{\text{ail}}^3k_{FB}\lambda_{FO_{rb}}^3 \cdots \end{aligned}$$

One can now relate the low-order (eq. (8)) and full-order, closed-loop rigid-body pole as

$$\begin{aligned} \lambda_{LO} = &\lambda_{FO_{rb}} + L_{\delta_{\text{ail}}}\tau_{\text{ail}}k_{FB}\lambda_{FO_{rb}} \\ &- L_{\delta_{\text{ail}}}\tau_{\text{ail}}^2k_{FB}\lambda_{FO_{rb}}^2 + L_{\delta_{\text{ail}}}\tau_{\text{ail}}^3k_{FB}\lambda_{FO_{rb}}^3 \cdots \end{aligned}$$

This is an infinite series that converges as long as

$$|\tau_{\text{ail}}\lambda_{FO_{rb}}| < 1$$

In the case where the actuator has a much lower time constant than the rigid-body mode $|\tau_{\text{ail}}\lambda_{FO_{rb}}| \ll 1$, the first two terms constitute a good approximation to the infinite series such that

$$\lambda_{LO} \approx \left(1 + L_{\delta_{\text{ail}}}\tau_{\text{ail}}k_{FB}\right)\lambda_{FO_{rb}}$$

or

$$\lambda_{FO_{rb}} \approx \widehat{\lambda}_{FO_{rb}} \equiv \left(1 + L_{\delta_{\text{ail}}}\tau_{\text{ail}}k_{FB}\right)^{-1}\lambda_{LO}$$

where $\widehat{\lambda}_{FO_{rb}}$ denotes an approximation of $\lambda_{FO_{rb}}$. A plot of this approximation is shown in figure 7. Note that $\widehat{\lambda}_{FO_{rb}}$ approximates $\lambda_{FO_{rb}}$ up to an actuator time constant of approximately 0.06 sec, which is three times slower than the actual actuator time constant.

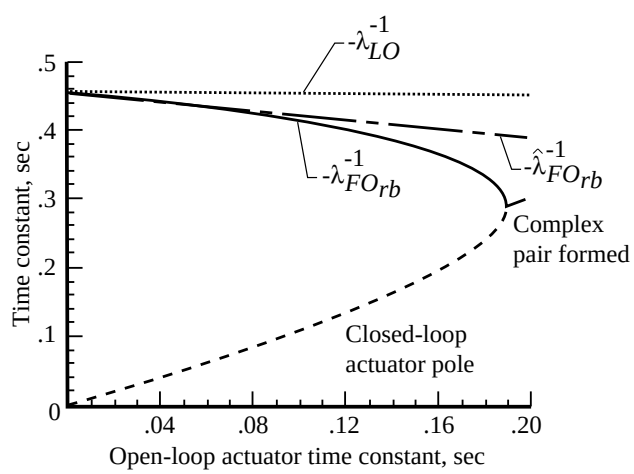

Figure 7. Effect of first-order actuator model on SISO system and approximation.

Because of the divergence of λ_{LO}^{-1} and $\lambda_{FO_{rb}}^{-1}$, a point will exist where the open-loop actuator time constant is high enough that it becomes necessary to include this actuator model in the design process. This point will be determined by the required level of accuracy in the final design. A point will also exist where the rigid-body roll mode and the actuator

mode couple together to form a single oscillatory mode.

Approximating the Transformation

First-Order Actuators

In this section, an approximation of the eigenspace transformation is derived and tested for unmodeled dynamics placed at the input of the rigid-body aircraft. The eigenspace transformation relates the rigid-body eigenspace of the low-order, closed-loop system used for the design with the full-order, closed-loop system. Here, the SISO results shown in the section entitled "SISO Example" are generalized for first-order lag actuator dynamics applied to the MIMO design.

Without feed-through term. Consider the following system, shown in figure 8, which represents the HARV rigid-body system and the first-order lag actuator models:

$$\begin{aligned} \dot{\mathbf{x}} &= \mathbf{A}\mathbf{x} + \mathbf{B}\mathbf{v} && \text{(System dynamics)} \\ \mathbf{z} &= \mathbf{M}\mathbf{x} && \text{(System measurements)} \\ \mathbf{T}_e\dot{\mathbf{v}} &= -\mathbf{v} + \mathbf{u} && \text{(Actuator dynamics)} \\ \mathbf{u} &= \mathbf{K}\mathbf{G}\mathbf{z} + \mathbf{K}\mathbf{u}_{\text{pilot}} && \text{(Control law)} \end{aligned} \tag{13}$$

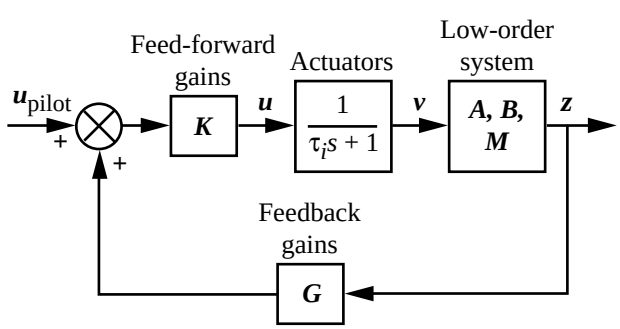

Figure 8. System block diagram with first-order lag actuators as unmodeled dynamics.

The measurement feed-through term is omitted from this derivation for clarity. The actuator matrix is diagonal and contains the time constant associated with each actuator:

$$\mathbf{T}_e \equiv \begin{bmatrix} \tau_1 & & 0 \\ & \ddots & \\ 0 & & \tau_e \end{bmatrix}$$

This formulation corresponds to actuator dynamics with the transfer functions

$$\frac{v_i(s)}{u_i(s)} = \frac{1}{\tau_i s + 1} \qquad (i = 1, 2, \ldots, e)$$

This full-order, closed-loop system now has $n + e$ states with dynamics expressed as

$$\begin{Bmatrix} \dot{\mathbf{x}} \\ \dot{\mathbf{v}} \end{Bmatrix} = \begin{bmatrix} \mathbf{A} & \mathbf{B} \\ \mathbf{T}_e^{-1}\mathbf{K}\mathbf{G}\mathbf{M} & -\mathbf{T}_e^{-1} \end{bmatrix} \begin{Bmatrix} \mathbf{x} \\ \mathbf{v} \end{Bmatrix} + \begin{bmatrix} 0 \\ \mathbf{T}_e^{-1}\mathbf{K} \end{bmatrix} \mathbf{u}_{\text{pilot}}$$

$$\mathbf{z} = [\mathbf{M} \;\; 0] \begin{Bmatrix} \mathbf{x} \\ \mathbf{v} \end{Bmatrix}$$

The closed-loop stability matrix for the low-order system is

$$\mathbf{A}_{LO} = \mathbf{A} + \mathbf{B}\mathbf{K}\mathbf{G}\mathbf{M}$$

and the closed-loop stability matrix for this full-order system is

$$\mathbf{A}_{FO} = \begin{bmatrix} \mathbf{A} & \mathbf{B} \\ \mathbf{T}_e^{-1}\mathbf{K}\mathbf{G}\mathbf{M} & -\mathbf{T}_e^{-1} \end{bmatrix}$$

Of interest are the eigenvectors and eigenvalues of this closed-loop system corresponding to the rigid-body dynamics. These correspond to $\mathbf{V}_{11}$ and $\mathbf{\Lambda}_1$ when this full-order system matrix is rewritten as the spectral decomposition,

$$\begin{bmatrix} \mathbf{A} & \mathbf{B} \\ \mathbf{T}_e^{-1}\mathbf{K}\mathbf{G}\mathbf{M} & -\mathbf{T}_e^{-1} \end{bmatrix} \begin{bmatrix} \mathbf{V}_{11} & \mathbf{V}_{12} \\ \mathbf{V}_{21} & \mathbf{V}_{22} \end{bmatrix} = \begin{bmatrix} \mathbf{V}_{11} & \mathbf{V}_{12} \\ \mathbf{V}_{21} & \mathbf{V}_{22} \end{bmatrix} \begin{bmatrix} \mathbf{\Lambda}_1 & 0 \\ 0 & \mathbf{\Lambda}_2 \end{bmatrix} \tag{14}$$

Here, we need only the upper left and lower left partitions of the above matrix equation, or

$$\mathbf{A}\mathbf{V}_{11} + \mathbf{B}\mathbf{V}_{21} = \mathbf{V}_{11}\mathbf{\Lambda}_1 \tag{15}$$

$$\mathbf{T}_e^{-1}\mathbf{K}\mathbf{G}\mathbf{M}\mathbf{V}_{11} - \mathbf{T}_e^{-1}\mathbf{V}_{21} = \mathbf{V}_{21}\mathbf{\Lambda}_1 \tag{16}$$

or equivalently,

$$\mathbf{V}_{11}\mathbf{\Lambda}_1 - \mathbf{A}\mathbf{V}_{11} = \mathbf{B}\mathbf{V}_{21} \tag{17}$$

$$\mathbf{K}\mathbf{G}\mathbf{M}\mathbf{V}_{11} = \mathbf{V}_{21} + \mathbf{T}_e\mathbf{V}_{21}\mathbf{\Lambda}_1 \tag{18}$$

As an intermediate step to obtain the eigenspace transformation approximation, equation (17) is expanded as an infinite series. To generate this series, add and subtract $\mathbf{B}\mathbf{T}_e\mathbf{V}_{21}\mathbf{\Lambda}_1$ and group terms corresponding to the right-hand side of equation (18). This becomes

$$\mathbf{V}_{11}\mathbf{\Lambda}_1 - \mathbf{A}\mathbf{V}_{11} = \mathbf{B}(\mathbf{V}_{21} + \mathbf{T}_e\mathbf{V}_{21}\mathbf{\Lambda}_1) - \mathbf{B}\mathbf{T}_e\mathbf{V}_{21}\mathbf{\Lambda}_1$$

Then add and subtract $\mathbf{B}\mathbf{T}_e^2\mathbf{V}_{21}\mathbf{\Lambda}_1^2$ and group as before such that

$$\begin{aligned} \mathbf{V}_{11}\mathbf{\Lambda}_1 - \mathbf{A}\mathbf{V}_{11} = \mathbf{B}(\mathbf{V}_{21} + \mathbf{T}_e\mathbf{V}_{21}\mathbf{\Lambda}_1) - \mathbf{B}\mathbf{T}_e(\mathbf{V}_{21} \\ + \mathbf{T}_e\mathbf{V}_{21}\mathbf{\Lambda}_1)\mathbf{\Lambda}_1 + \mathbf{B}\mathbf{T}_e^2\mathbf{V}_{21}\mathbf{\Lambda}_1^2 \end{aligned}$$

where $\mathbf{A}^2 \equiv \mathbf{AA}$, $\mathbf{A}^3 \equiv \mathbf{AAA}, \ldots$ Continuing to add and subtract $\mathbf{BT}_e^i\mathbf{V}_{21}\mathbf{\Lambda}_1^i$ $(i = 3, 4, \ldots, \infty)$ and following the same grouping strategy yields the following infinite series:

$$\begin{aligned}\mathbf{V}_{11}\mathbf{\Lambda}_1 - \mathbf{AV}_{11} = {} & \mathbf{B}(\mathbf{V}_{21} + \mathbf{T}_e\mathbf{V}_{21}\mathbf{\Lambda}_1) \\ & - \mathbf{BT}_e(\mathbf{V}_{21} + \mathbf{T}_e\mathbf{V}_{21}\mathbf{\Lambda}_1)\mathbf{\Lambda}_1 \\ & + \mathbf{BT}_e^2(\mathbf{V}_{21} + \mathbf{T}_e\mathbf{V}_{21}\mathbf{\Lambda}_1)\mathbf{\Lambda}_1^2 \\ & - \mathbf{BT}_e^3(\mathbf{V}_{21} + \mathbf{T}_e\mathbf{V}_{21}\mathbf{\Lambda}_1)\mathbf{\Lambda}_1^3 + \ldots\end{aligned}$$

Equation (18) can now be substituted into each term on the right to get

$$\begin{aligned}\mathbf{V}_{11}\mathbf{\Lambda}_1 - \mathbf{AV}_{11} = {} & \mathbf{BKGMV}_{11} - \mathbf{BT}_e\mathbf{KGMV}_{11}\mathbf{\Lambda}_1 \\ & + \mathbf{BT}_e^2\mathbf{KGMV}_{11}\mathbf{\Lambda}_1^2 - \ldots \qquad (19)\end{aligned}$$

Postmultiply equation (19) by $\mathbf{V}_{11}^{-1}$. The infinite series that results relates the rigid-body eigenspace of the low-order, closed-loop system with that of the full-order, closed-loop system in which

$$\begin{aligned}\mathbf{A}_{LO} = {} & (\mathbf{A}_{FO})_{rb} + \mathbf{BT}_e\mathbf{KGM}(\mathbf{A}_{FO})_{rb} \\ & - \mathbf{BT}_e^2\mathbf{KGM}(\mathbf{A}_{FO})_{rb}^2 \\ & + \mathbf{BT}_e^3\mathbf{KGM}(\mathbf{A}_{FO})_{rb}^3 - \ldots \qquad (20)\end{aligned}$$

where

$$(\mathbf{A}_{FO})_{rb} = \mathbf{V}_{11}\mathbf{\Lambda}_1\mathbf{V}_{11}^{-1}$$

as defined in the section entitled "Spectral Decomposition."

As the amount of augmentation increases ($\mathbf{K}$ and $\mathbf{G}$), the effect of the unmodeled dynamics on the rigid-body dynamics is increased. As the actuators get faster (i.e., as the elements of $\mathbf{T}_e$ approach 0) the effect on the closed-loop eigenspace is decreased. The eigenspace of the low-order, closed-loop system and the rigid-body eigenspace of the full-order, closed-loop system become equal.

The convergence of equation (19) is equivalent to the convergence of

$$\sum_{i=0}^{\infty}(-1)^i\mathbf{T}_e^i\mathbf{KGMV}_{11}\mathbf{\Lambda}_1^i$$

This series can be bounded using the matrix 2-norm and the Schwarz inequality (ref. 8) such that

$$\|\mathbf{T}_e^i\mathbf{KGMV}_{11}\mathbf{\Lambda}_1^i\| \le \|\mathbf{T}_e\|^i\|\mathbf{KGMV}_{11}\|\,\|\mathbf{\Lambda}_1\|^i \qquad (i = 0, 1, \ldots, \infty)$$

The matrix 2-norm of $\mathbf{A}$ equals $\max\lambda(\mathbf{AA}^*)^{1/2}$. By virtue of being eigenvectors, $\mathbf{V}_{11}$ can be multiplied by an arbitrary scalar. This factor is chosen such that the matrix norm of $\mathbf{KGMV}_{11}$ is unity, so that

$$\|\mathbf{T}_e^i\mathbf{KGMV}_{11}\mathbf{\Lambda}_1^i\| \le (\|\mathbf{T}_e\|\,\|\mathbf{\Lambda}_1\|)^i$$

Convergence of equation (19) is therefore guaranteed when

$$\|\mathbf{T}_e\|\,\|\mathbf{\Lambda}_1\| < 1$$

Feed-through term. For many systems, the low-order model of interest may have a feed-through or $\mathbf{N}$ matrix term. This is the case for the HARV control law design. Here, the previous analysis and the development are extended to obtain the eigenspace transformation matrix for this type system. To begin, consider the system that represents an aircraft with first-order lag actuator models in which

$$\begin{aligned}\dot{\mathbf{x}} &= \mathbf{Ax} + \mathbf{Bv} && \text{(System dynamics)} \\ \mathbf{z} &= \mathbf{Mx} + \mathbf{Nv} && \text{(System measurements)} \\ \mathbf{T}_e\dot{\mathbf{v}} &= -\mathbf{v} + \mathbf{u} && \text{(Actuator dynamics)} \\ \mathbf{u} &= \mathbf{KGz} + \mathbf{Ku}_{\text{pilot}} && \text{(Control law)}\end{aligned}$$

The system has $n + e$ states, with the closed-loop dynamics

$$\begin{aligned}\begin{Bmatrix}\dot{\mathbf{x}} \\ \dot{\mathbf{v}}\end{Bmatrix} &= \begin{bmatrix}\mathbf{A} & \mathbf{B} \\ \mathbf{T}_e^{-1}\mathbf{KGM} & \mathbf{T}_e^{-1}\mathbf{KGN} - \mathbf{T}_e^{-1}\end{bmatrix}\begin{Bmatrix}\mathbf{x} \\ \mathbf{v}\end{Bmatrix} \\ &\quad + \begin{bmatrix}0 \\ \mathbf{T}_e^{-1}\mathbf{K}\end{bmatrix}\mathbf{u}_{\text{pilot}} \\ \mathbf{z} &= [\mathbf{M} \;\; \mathbf{N}]\begin{Bmatrix}\mathbf{x} \\ v\end{Bmatrix}\end{aligned}$$

The spectral decomposition of the system matrix is

$$\begin{aligned}&\begin{bmatrix}\mathbf{A} & \mathbf{B} \\ \mathbf{T}_e^{-1}\mathbf{KGM} & \mathbf{T}_e^{-1}\mathbf{KGN} - \mathbf{T}_e^{-1}\end{bmatrix}\begin{bmatrix}\mathbf{V}_{11} & \mathbf{V}_{12} \\ \mathbf{V}_{21} & \mathbf{V}_{22}\end{bmatrix} \\ &\quad = \begin{bmatrix}\mathbf{V}_{11} & \mathbf{V}_{12} \\ \mathbf{V}_{21} & \mathbf{V}_{22}\end{bmatrix}\begin{bmatrix}\mathbf{\Lambda}_1 & 0 \\ 0 & \mathbf{\Lambda}_2\end{bmatrix}\end{aligned}$$

where $\mathbf{\Lambda}_1$ and $\mathbf{V}_{11}$ correspond to the rigid-body eigenspace. As before, only the upper left and lower left partitions of this equation are used, or

$$\mathbf{V}_{11}\mathbf{\Lambda}_1 - \mathbf{AV}_{11} = \mathbf{BV}_{21} \qquad (21)$$

$$\mathbf{KGMV}_{11} = \mathbf{Q}_e\mathbf{V}_{21} + \mathbf{T}_e\mathbf{V}_{21}\mathbf{\Lambda}_1 \qquad (22)$$

where

$$\mathbf{Q}_e \equiv \mathbf{I} - \mathbf{KGN}$$

This is a useful definition for the development to follow, since from the section entitled "Low-Order, Closed-Loop System"

$$\mathbf{A}_{LO} = \mathbf{A} + \mathbf{B}\mathbf{Q}_e^{-1}\mathbf{K}\mathbf{G}\mathbf{M}$$

As in the previous section, equation (21) is expanded as an infinite series with terms grouped to match the right-hand side of equation (22). The series is generated as before: add and subtract $\mathbf{B}\mathbf{Q}_e^{-1}\mathbf{T}_e\mathbf{V}_{21}\mathbf{\Lambda}_1$ to equation (21), so that

$$\mathbf{V}_{11}\mathbf{\Lambda}_1 - \mathbf{A}\mathbf{V}_{11} = \mathbf{B}\mathbf{Q}_e^{-1}(\mathbf{Q}_e\mathbf{V}_{21} + \mathbf{T}_e\mathbf{V}_{21}\mathbf{\Lambda}_1) - \mathbf{B}\mathbf{Q}_e^{-1}\mathbf{T}_e\mathbf{V}_{21}\mathbf{\Lambda}_1$$

Then continue in a similar manner as before and apply equation (22) as follows:

$$\mathbf{V}_{11}\mathbf{\Lambda}_1 - \mathbf{A}\mathbf{V}_{11} = \mathbf{B}\mathbf{K}\mathbf{G}\mathbf{M}\mathbf{V}_{11} - \mathbf{B}\mathbf{Q}_e^{-1}\mathbf{T}_e\mathbf{Q}_e^{-1}\mathbf{K}\mathbf{G}\mathbf{M}\mathbf{V}_{11}\mathbf{\Lambda}_1 + \mathbf{B}\mathbf{Q}_e^{-1}\mathbf{T}_e\mathbf{Q}_e^{-1}\mathbf{T}_e\mathbf{Q}_e^{-1}\mathbf{K}\mathbf{G}\mathbf{M}\mathbf{V}_{11}\mathbf{\Lambda}_1^2 - \ldots$$

Convergence is guaranteed when $\|\mathbf{Q}_e^{-1}\mathbf{T}_e\|\,\|\mathbf{\Lambda}_1\| < 1$. To obtain the final form, postmultiply by $\mathbf{V}_{11}^{-1}$, so that

$$\mathbf{A}_{LO} = (\mathbf{A}_{FO})_{rb} + \mathbf{B}\mathbf{Q}_e^{-1}\mathbf{T}_e\mathbf{Q}_e^{-1}\mathbf{K}\mathbf{G}\mathbf{M}(\mathbf{A}_{FO})_{rb} - \mathbf{B}\mathbf{Q}_e^{-1}\mathbf{T}_e\mathbf{Q}_e^{-1}\mathbf{T}_e\mathbf{Q}_e^{-1}\mathbf{K}\mathbf{G}\mathbf{M}(\mathbf{A}_{FO})_{rb}^2 + \ldots \quad (23)$$

An important simplification of equation (23) is suggested by multiplying through by $(\mathbf{A}_{FO})_{rb}^{-1}$, so that

$$\mathbf{A}_{LO}(\mathbf{A}_{FO})_{rb}^{-1} = \mathbf{I} + \mathbf{B}\mathbf{Q}_e^{-1}\mathbf{T}_e\mathbf{Q}_e^{-1}\mathbf{K}\mathbf{G}\mathbf{M} - \mathbf{B}\mathbf{Q}_e^{-1}\mathbf{T}_e\mathbf{Q}_e^{-1}\mathbf{T}_e\mathbf{Q}_e^{-1}\mathbf{K}\mathbf{G}\mathbf{M}(\mathbf{A}_{FO})_{rb} + \ldots$$

The 2-norm of each successive term on the right-hand side, except the identity term, is shown in figure 9. Clearly, the first two terms constitute a reasonable approximation to the infinite series for this example.

An advantage of using the first two terms as an approximation to the series is the following prediction of the rigid-body eigenspace of the full-order, closed-loop system expressed in terms of the low-order, closed-loop system:

$$(\mathbf{A}_{FO})_{rb} \approx (\mathbf{I} + \mathbf{B}\mathbf{Q}_e^{-1}\mathbf{T}_e\mathbf{Q}_e^{-1}\mathbf{K}\mathbf{G}\mathbf{M})^{-1}\mathbf{A}_{LO}$$

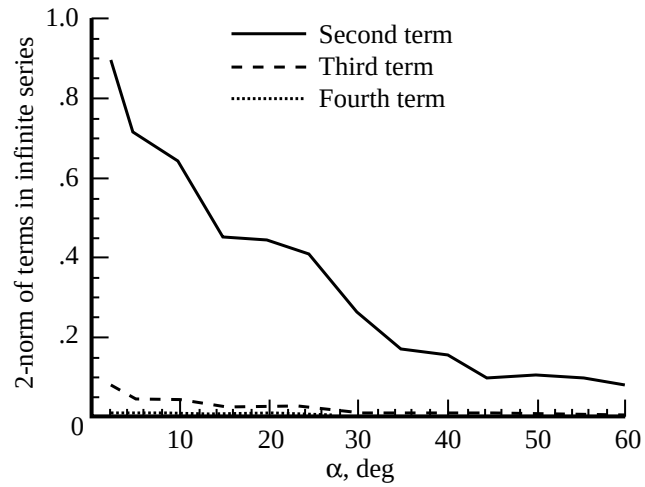

Figure 9. 2-norm of terms in infinite series.

This expression leads to the concept of a single matrix (an eigenspace transformation matrix) which transforms the low-order, closed-loop stability matrix to approximate the rigid-body eigenspace of the full-order, closed-loop system such that

$$(\mathbf{A}_{FO})_{rb} \approx \mathbf{E}^{-1}\mathbf{A}_{LO} \quad (24)$$

For this full-order, closed-loop system, the eigenspace transformation matrix is simply

$$\mathbf{E} = \mathbf{I} + \mathbf{B}\mathbf{Q}_e^{-1}\mathbf{T}_e\mathbf{Q}_e^{-1}\mathbf{K}\mathbf{G}\mathbf{M}$$

Application

The results of the previous development are applied to the HARV lateral-directional flight control system design. The validity of the previous analysis in predicting the effect of first-order actuator models on the rigid-body dynamics is shown. The low-order system was used to generate the feedback gains. Because there are four measurements, the rigid-body poles are exactly placed. Moreover, the low-order, closed-loop eigenspace is the desired eigenspace.

In this example, the actuators are modeled as the following transfer functions:

$$TF_{\text{ail}}(s) = \frac{1}{\frac{1}{48}s + 1} \qquad TF_{\text{rud}}(s) = \frac{1}{\frac{1}{40}s + 1}$$

$$TF_{as}(s) = \frac{1}{\frac{1}{30}s + 1} \qquad TF_{\text{ytv}}(s) = \frac{1}{\frac{1}{48}s + 1}$$

$$TF_{\text{rtv}}(s) = \frac{1}{\frac{1}{48}s + 1}$$

The approximate eigenspace transformation matrix is then

$$\mathbf{E} = \mathbf{I} + \mathbf{B}\mathbf{Q}_e^{-1} \begin{bmatrix} \frac{1}{48} & & & & 0 \\ & \frac{1}{40} & & & \\ & & \frac{1}{30} & & \\ & & & \frac{1}{48} & \\ 0 & & & & \frac{1}{48} \end{bmatrix} \mathbf{Q}_e^{-1}\mathbf{K}\mathbf{G}\mathbf{M} \tag{25}$$

The expression $\mathbf{E}^{-1}\mathbf{A}_{LO}$ is postulated to be an approximation to the rigid-body eigenspace of the full-order, closed-loop system (i.e., $\mathbf{V}_{11}\mathbf{\Lambda}_1\mathbf{V}_{11}^{-1}$).

The first check on the validity of the approximation will be on the convergence of the infinite series used to derive the eigenspace transformation matrix. The test

$$\|\mathbf{Q}_e^{-1}\mathbf{T}_e\| \, \|\mathbf{\Lambda}_1 < 1$$

is applied using the 2-norm. At an angle of attack of 20°, the left side of the equation is equal to 0.0737. This value indicates convergence of the series.

To examine the range in which the eigenspace transformation matrix is valid, the poles of the actuators are gradually slowed down. This procedure is done by multiplying the actuator poles by a reduction factor k which is varied from 1 to 0 such that

$$\mathbf{T}_{\text{slow}}^{-1} = k\mathbf{T}_e^{-1}$$

where

$$\mathbf{T}_{\text{slow}}\dot{\mathbf{v}} = -\mathbf{v} + \mathbf{u}$$

The error associated with using this eigenspace transformation matrix in predicting the roll mode pole and Dutch roll natural frequency for a flight condition with an angle of attack of 20° is shown in figure 10. The actuators have been slowed by a factor of 5 when the aileron actuator and the roll mode poles form an oscillatory pair. The unmodeled dynamics will need to be much closer in frequency to the low-order, closed-loop system for there to be a problem with the assumptions made.

Figure 11 shows how well $\mathbf{E}^{-1}\mathbf{A}_{LO}$ predicts the rigid-body roll mode pole. The low-order characteristics are those of the design model, and they represent placed dynamics. The full-order characteristics are those of the low-order plant plus the actuator dynamics. The predicted characteristics are obtained from equation (24), and they are expected to predict the full-order characteristics. The Dutch roll mode pole is shown in figure 12. Note that the variation of the roll mode and Dutch roll frequencies are captured along with the variation in Dutch roll damping. The

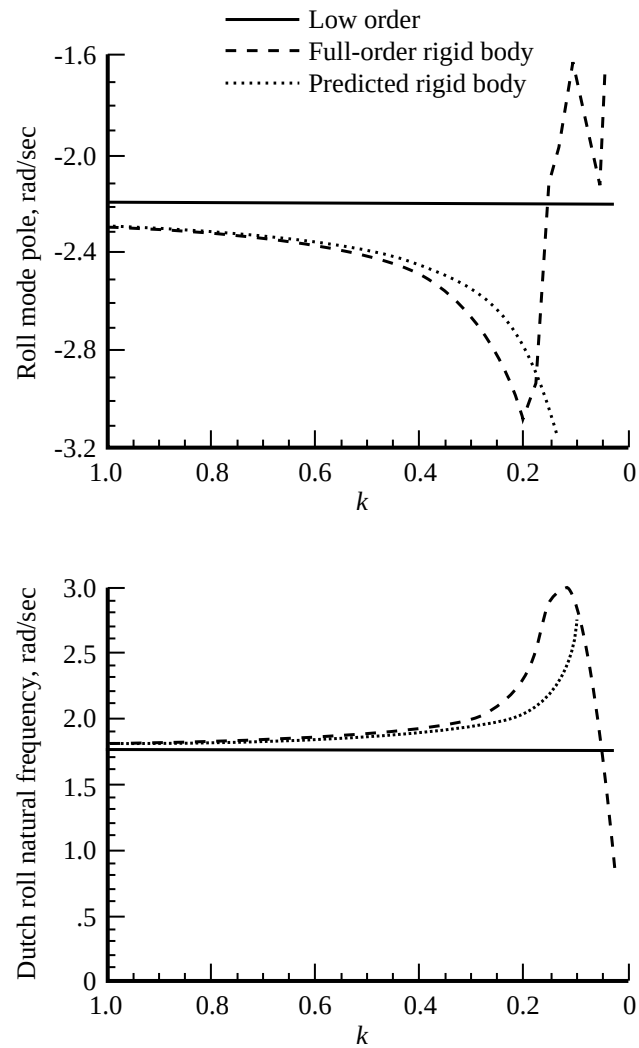

Figure 10. Plots that verify accuracy of eigenspace transformation matrix approximation with angle of attack of 20°.

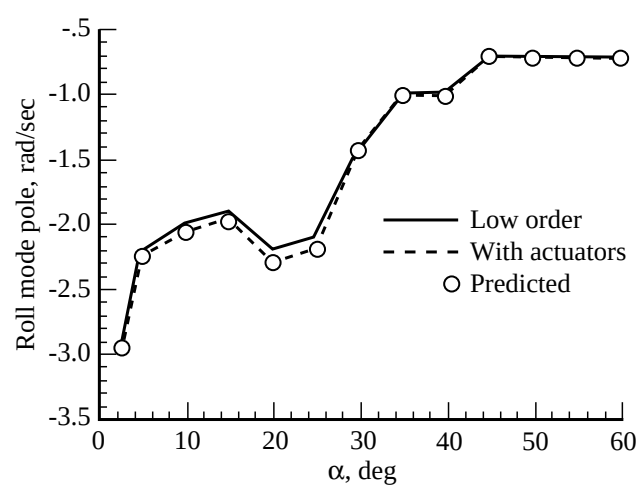

Figure 11. Roll mode pole prediction with actuator models.

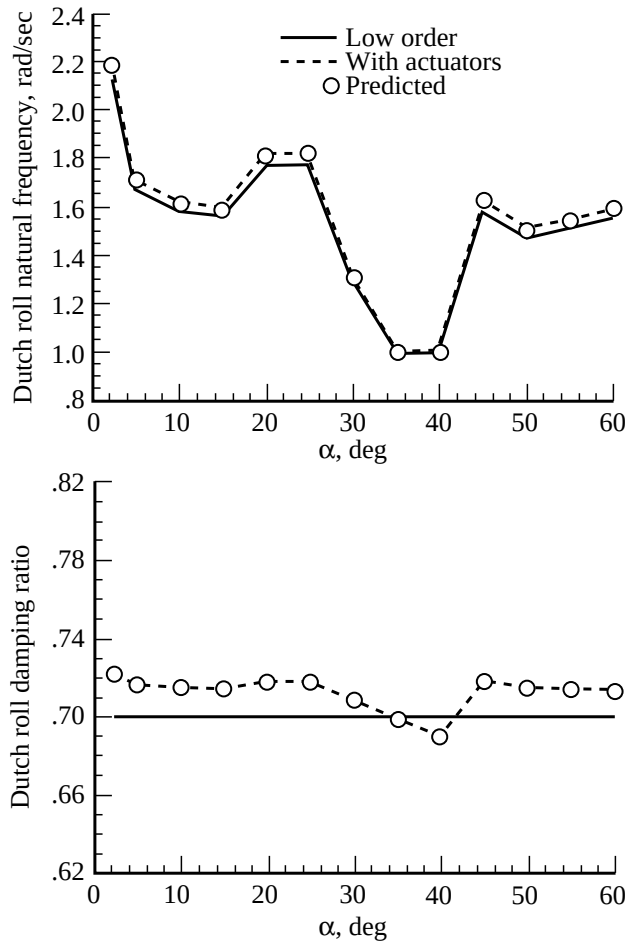

Figure 12. Dutch roll mode pole prediction with actuator models.

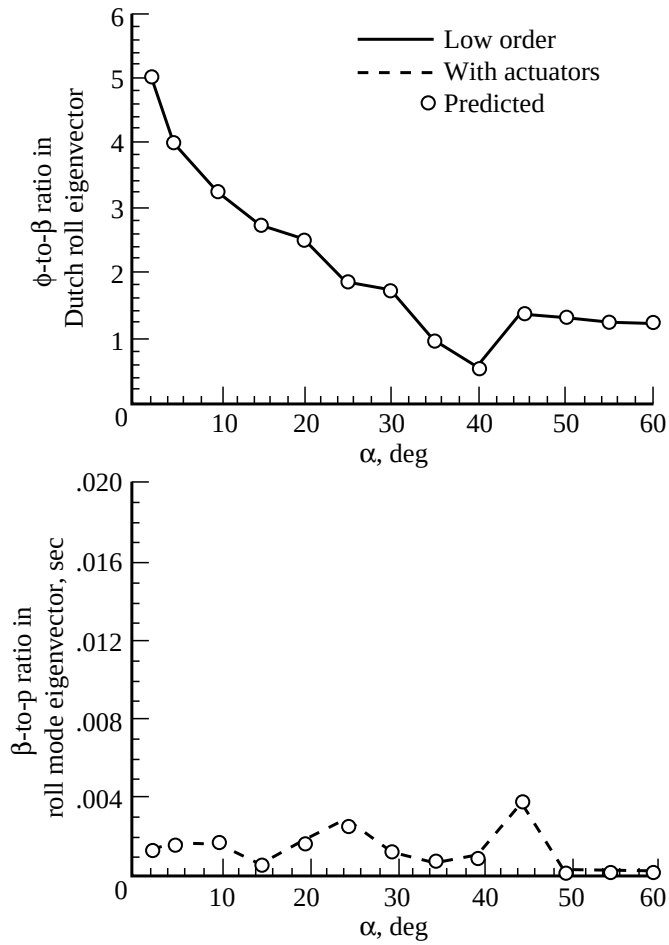

Figure 13. Eigenvector prediction with actuator models.

negligible variation of the spiral mode pole, which is not shown, is also captured by the approximation. For all cases, the approximate eigenspace transformation matrix accurately predicts the rigid-body poles of the full-order, closed-loop system.

The predicted effect of actuators on the desired eigenvector elements is shown in figure 13. The first of these elements is the ϕ-to-β ratio in the Dutch roll mode. The second element is the β-to-p ratio in the roll mode. The magnitude of the ratio of each of these two eigenvector elements is shown. These ratios give an indication of how much the roll and Dutch roll modes are coupled. The low-order β-to-p ratio in the roll mode is 0 for all cases. The low-order ϕ-to-β ratio in the Dutch roll mode coincides with that of the full-order, closed-loop system. The β-to-p ratio is in seconds, and the ϕ-to-β ratio is nondimensional. The eigenvectors appear to be affected considerably less than the eigenvalues by unmodeled dynamics. This result will show up repeatedly in the examples that are presented. Again, the approximate eigenspace transformation matrix accurately predicts the full-order, closed-loop rigid-body eigenspace.

Dynamics in Other Locations

General Form of Eigenspace Transformation Matrix

One would like a general expression for the eigenspace transformation matrix for dynamics at other points, including the input to the plant, in the control system structure. It is possible to construct the system with a first-order lag at three locations within this system. The eigenspace transformation matrix for a first-order lag in any or all of these locations will then be readily available from the general form.

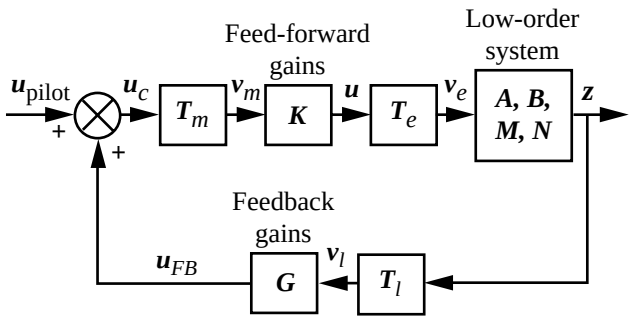

Figure 14. System block diagram with first-order lags in three locations.

Consider the system shown in figure 14, in which

$$\begin{aligned}
\dot{\mathbf{x}} &= \mathbf{A}\mathbf{x} + \mathbf{B}\mathbf{v}_e & \mathbf{T}_e\dot{\mathbf{v}}_e &= -\mathbf{v}_e + \mathbf{u} \\
\mathbf{u} &= \mathbf{K}\mathbf{v}_m & \mathbf{T}_m\dot{\mathbf{v}}_m &= -\mathbf{v}_m + \mathbf{u}_c \\
\mathbf{u}_{FB} &= \mathbf{G}\mathbf{v}_l & \mathbf{T}_l\dot{\mathbf{v}}_l &= -\mathbf{v}_l + \mathbf{z} \\
\mathbf{z} &= \mathbf{M}\mathbf{x} + \mathbf{N}\mathbf{v}_e & \mathbf{u}_c &= \mathbf{u}_{FB} + \mathbf{u}_{\text{pilot}}
\end{aligned}$$

where $\mathbf{x} \in \underline{R}^n$, $v_e \in \underline{R}^e$, $v_m \in \underline{R}^m$, and $v_l \in \underline{R}^l$. When the equations governing this system are combined, the full-order, closed-loop system becomes

$$\begin{Bmatrix} \dot{\mathbf{x}} \\ \dot{\mathbf{v}}_e \\ \dot{\mathbf{v}}_m \\ \dot{\mathbf{v}}_l \end{Bmatrix} = \begin{bmatrix} \mathbf{A} & \mathbf{B} & 0 & 0 \\ 0 & -\mathbf{T}_e^{-1} & \mathbf{T}_e^{-1}\mathbf{K} & 0 \\ 0 & 0 & -\mathbf{T}_m^{-1} & \mathbf{T}_m^{-1}\mathbf{G} \\ \mathbf{T}_l^{-1}\mathbf{M} & \mathbf{T}_l^{-1}\mathbf{N} & 0 & -\mathbf{T}_l^{-1} \end{bmatrix} \begin{Bmatrix} \mathbf{x} \\ \mathbf{v}_e \\ \mathbf{v}_m \\ \mathbf{v}_l \end{Bmatrix}$$

$$+ \begin{Bmatrix} 0 \\ 0 \\ \mathbf{T}_m^{-1} \\ 0 \end{Bmatrix} \mathbf{u}_{\text{pilot}}$$

with $n+e+m+l$ states. The spectral decomposition of the system matrix becomes

$$\begin{bmatrix} \mathbf{A} & \mathbf{B} & 0 & 0 \\ 0 & -\mathbf{T}_e^{-1} & \mathbf{T}_e^{-1}\mathbf{K} & 0 \\ 0 & 0 & -\mathbf{T}_m^{-1} & \mathbf{T}_m^{-1}\mathbf{G} \\ \mathbf{T}_l^{-1}\mathbf{M} & \mathbf{T}_l^{-1}\mathbf{N} & 0 & -\mathbf{T}_l^{-1} \end{bmatrix} \begin{bmatrix} \mathbf{V}_{11} & \mathbf{V}_{12} \\ \mathbf{V}_{21} & \mathbf{V}_{22} \\ \mathbf{V}_{31} & \mathbf{V}_{32} \\ \mathbf{V}_{41} & \mathbf{V}_{42} \end{bmatrix}$$

$$= \begin{bmatrix} \mathbf{V}_{11} & \mathbf{V}_{12} \\ \mathbf{V}_{21} & \mathbf{V}_{22} \\ \mathbf{V}_{31} & \mathbf{V}_{32} \\ \mathbf{V}_{41} & \mathbf{V}_{42} \end{bmatrix} \begin{bmatrix} \mathbf{\Lambda}_1 & 0 \\ 0 & \mathbf{\Lambda}_2 \end{bmatrix} \tag{26}$$

where $\mathbf{V}_{11}$ and $\mathbf{\Lambda}_1$ are the eigenvector elements and eigenvalues associated with the rigid-body eigenspace of the full-order, closed-loop system, respectively. The eigenvector matrix has been partitioned such that the first-column partition contains n columns, and the second contains $e+m+l$ columns. The first-, second-, third-, and fourth-row partitions contain n, e, m, and l rows, respectively. Equations in the first-column partition of the matrix equation (26) are

$$\mathbf{V}_{11}\mathbf{\Lambda}_1 - \mathbf{A}\mathbf{V}_{11} = \mathbf{B}\mathbf{V}_{21} \tag{27}$$

$$\mathbf{K}\mathbf{V}_{31} = \mathbf{V}_{21} + \mathbf{T}_p\mathbf{V}_{21}\mathbf{\Lambda}_1 \tag{28}$$

$$\mathbf{G}\mathbf{V}_{41} = \mathbf{V}_{31} + \mathbf{T}_m\mathbf{V}_{31}\mathbf{\Lambda}_1 \tag{29}$$

$$\mathbf{M}\mathbf{V}_{11} = -\mathbf{N}\mathbf{V}_{21} + \mathbf{V}_{41} + \mathbf{T}_l\mathbf{V}_{41}\mathbf{\Lambda}_1 \tag{30}$$

To get the feed-through term in a useful form, a second version of equations (28), (29), and (30) is needed, so that

$$\mathbf{K}\mathbf{V}_{31} = \mathbf{Q}_e\mathbf{V}_{21} + \mathbf{T}_e\mathbf{V}_{21}\mathbf{\Lambda}_1 + \mathbf{K}\mathbf{G}\mathbf{N}\mathbf{V}_{21} \tag{31}$$

$$\mathbf{G}\mathbf{V}_{41} = \mathbf{Q}_m\mathbf{V}_{31} + \mathbf{T}_m\mathbf{V}_{31}\mathbf{\Lambda}_1 + \mathbf{G}\mathbf{N}\mathbf{K}\mathbf{V}_{31} \tag{32}$$

$$\mathbf{M}\mathbf{V}_{11} = \mathbf{Q}_l\mathbf{V}_{41} + \mathbf{T}_l\mathbf{V}_{41}\mathbf{\Lambda}_1 + \mathbf{N}\mathbf{K}\mathbf{G}\mathbf{V}_{41} - \mathbf{N}\mathbf{V}_{21} \tag{33}$$

where

$$\mathbf{Q}_e \equiv \mathbf{I} - \mathbf{K}\mathbf{G}\mathbf{N}$$

$$\mathbf{Q}_m \equiv \mathbf{I} - \mathbf{G}\mathbf{N}\mathbf{K}$$

$$\mathbf{Q}_l \equiv \mathbf{I} - \mathbf{N}\mathbf{K}\mathbf{G}$$

As in the previous development, expansion obtained via adding and subtracting needed terms will turn equations (27) through (30) into an infinite series. It is again assumed that the speed of the unmodeled dynamics is faster than that of the low-order, closed-loop system. Hence, each new term of the series will be smaller than its predecessor. To form an analogous approximation to the series, all terms containing two or more time constant matrices and two or more eigenvalue matrices will be dropped. Expand equation (27) so that equation (31) can be used; thus,

$$\begin{aligned}
\mathbf{V}_{11}\mathbf{\Lambda}_1 - \mathbf{A}\mathbf{V}_{11} = {} & \mathbf{B}\mathbf{Q}_e^{-1}(\mathbf{Q}_e\mathbf{V}_{21} + \mathbf{T}_e\mathbf{V}_{21}\mathbf{\Lambda}_1) \\
& - \mathbf{B}\mathbf{Q}_e^{-1}\mathbf{T}_e\mathbf{Q}_e^{-1}(\mathbf{Q}_e\mathbf{V}_{21} + \mathbf{T}_e\mathbf{V}_{21}\mathbf{\Lambda}_1)\mathbf{\Lambda}_1 \\
& + \mathbf{B}\mathbf{Q}_e^{-1}\mathbf{T}_e\mathbf{Q}_e^{-1}\mathbf{T}_e\mathbf{Q}_e^{-1}(\mathbf{Q}_e\mathbf{V}_{21} \\
& + \mathbf{T}_e\mathbf{V}_{21}\mathbf{\Lambda}_1)\mathbf{\Lambda}_1^2 - \ldots
\end{aligned}$$

Then apply equation (31) and drop the terms with higher powers of $\mathbf{T}_e$ and $\mathbf{\Lambda}_1$, so that

$$\begin{aligned}
\mathbf{V}_{11}\mathbf{\Lambda}_1 - \mathbf{A}\mathbf{V}_{11} \approx {} & \mathbf{B}\mathbf{Q}_e^{-1}(\mathbf{K}\mathbf{V}_{31} - \mathbf{K}\mathbf{G}\mathbf{N}\mathbf{V}_{21}) \\
& - \mathbf{B}\mathbf{Q}_e^{-1}\mathbf{T}_e\mathbf{Q}_e^{-1}(\mathbf{K}\mathbf{V}_{31} - \mathbf{K}\mathbf{G}\mathbf{N}\mathbf{V}_{21})\mathbf{\Lambda}_1
\end{aligned}$$

For the remainder of the development, this equation will be stated as an approximation; all terms with

more than a single appearance of $\mathbf{T}$ and $\mathbf{\Lambda}_1$ will be dropped as they occur.

Expand the above equation again so that the right-hand side of equation (29) appears as

$$\begin{aligned}\mathbf{V}_{11}\mathbf{\Lambda}_1 - \mathbf{A}\mathbf{V}_{11} \approx\ & \mathbf{B}\mathbf{Q}_e^{-1}\mathbf{K}(\mathbf{V}_{31} + \mathbf{T}_m\mathbf{V}_{31}\mathbf{\Lambda}_1 - \mathbf{G}\mathbf{N}\mathbf{V}_{21}) \\ & - \mathbf{B}\mathbf{Q}_e^{-1}\mathbf{K}\mathbf{T}_m\mathbf{V}_{31}\mathbf{\Lambda}_1 \\ & - \mathbf{B}\mathbf{Q}_e^{-1}\mathbf{T}_e\mathbf{Q}_e^{-1}\mathbf{K}(\mathbf{V}_{31} + \mathbf{T}_m\mathbf{V}_{31}\mathbf{\Lambda}_1 \\ & - \mathbf{G}\mathbf{N}\mathbf{V}_{21})\mathbf{\Lambda}_1\end{aligned}$$

Then by equation (29),

$$\begin{aligned}\mathbf{V}_{11}\mathbf{\Lambda}_1 - \mathbf{A}\mathbf{V}_{11} \approx\ & \mathbf{B}\mathbf{Q}_e^{-1}\mathbf{K}(\mathbf{G}\mathbf{V}_{41} - \mathbf{G}\mathbf{N}\mathbf{V}_{21}) \\ & - \mathbf{B}\mathbf{Q}_e^{-1}\mathbf{K}\mathbf{T}_m\mathbf{V}_{31}\mathbf{\Lambda}_1 \\ & - \mathbf{B}\mathbf{Q}_e^{-1}\mathbf{T}_e\mathbf{Q}_e^{-1}\mathbf{K}(\mathbf{G}\mathbf{V}_{41} - \mathbf{G}\mathbf{N}\mathbf{V}_{21})\mathbf{\Lambda}_1\end{aligned}$$

Equation (32) will now be used to eliminate the last $\mathbf{V}_{31}$ term, so that

$$\begin{aligned}\mathbf{V}_{11}\mathbf{\Lambda}_1 - \mathbf{A}\mathbf{V}_{11} \approx\ & \mathbf{B}\mathbf{Q}_e^{-1}\mathbf{K}\mathbf{G}(\mathbf{V}_{41} - \mathbf{N}\mathbf{V}_{21}) \\ & - \mathbf{B}\mathbf{Q}_e^{-1}\mathbf{K}\mathbf{T}_m\mathbf{Q}_m^{-1}(\mathbf{Q}_m\mathbf{V}_{31} + \mathbf{T}_m\mathbf{V}_{31}\mathbf{\Lambda}_1)\mathbf{\Lambda}_1 \\ & - \mathbf{B}\mathbf{Q}_e^{-1}\mathbf{T}_e\mathbf{Q}_e^{-1}\mathbf{K}\mathbf{G}(\mathbf{V}_{41} - \mathbf{N}\mathbf{V}_{21})\mathbf{\Lambda}_1\end{aligned}$$

and then

$$\begin{aligned}\mathbf{V}_{11}\mathbf{\Lambda}_1 - \mathbf{A}\mathbf{V}_{11} \approx\ & \mathbf{B}\mathbf{Q}_e^{-1}\mathbf{K}\mathbf{G}(\mathbf{V}_{41} - \mathbf{N}\mathbf{V}_{21}) \\ & - \mathbf{B}\mathbf{Q}_e^{-1}\mathbf{K}\mathbf{T}_m\mathbf{Q}_m^{-1}\mathbf{G}(\mathbf{V}_{41} - \mathbf{N}\mathbf{K}\mathbf{V}_{31})\mathbf{\Lambda}_1 \\ & - \mathbf{B}\mathbf{Q}_e^{-1}\mathbf{T}_e\mathbf{Q}_e^{-1}\mathbf{K}\mathbf{G}(\mathbf{V}_{41} - \mathbf{N}\mathbf{V}_{21})\mathbf{\Lambda}_1\end{aligned}$$

Equation (28) is then used; thus,

$$\begin{aligned}\mathbf{V}_{11}\mathbf{\Lambda}_1 - \mathbf{A}\mathbf{V}_{11} \approx\ & \mathbf{B}\mathbf{Q}_e^{-1}\mathbf{K}\mathbf{G}(\mathbf{V}_{41} - \mathbf{N}\mathbf{V}_{21}) \\ & - \mathbf{B}\mathbf{Q}_e^{-1}\mathbf{K}\mathbf{T}_m\mathbf{Q}_m^{-1}\mathbf{G}(\mathbf{V}_{41} - \mathbf{N}\mathbf{V}_{21})\mathbf{\Lambda}_1 \\ & - \mathbf{B}\mathbf{Q}_e^{-1}\mathbf{T}_e\mathbf{Q}_e^{-1}\mathbf{K}\mathbf{G}(\mathbf{V}_{41} - \mathbf{N}\mathbf{V}_{21})\mathbf{\Lambda}_1\end{aligned}$$

Expand the above equation again so that the right-hand side of equation (30) will allow $\mathbf{V}_{41}$ to be eliminated:

$$\begin{aligned}\mathbf{V}_{11}\mathbf{\Lambda}_1 - \mathbf{A}\mathbf{V}_{11} \approx\ & \mathbf{B}\mathbf{Q}_e^{-1}\mathbf{K}\mathbf{G}(\mathbf{V}_{41} + \mathbf{T}_l\mathbf{V}_{41}\mathbf{\Lambda}_1 \\ & - \mathbf{N}\mathbf{V}_{21}) - \mathbf{B}\mathbf{Q}_e^{-1}\mathbf{K}\mathbf{G}\mathbf{T}_l\mathbf{V}_{41}\mathbf{\Lambda}_1 \\ & - \mathbf{B}\mathbf{Q}_e^{-1}\mathbf{K}\mathbf{T}_m\mathbf{Q}_m^{-1}\mathbf{G}(\mathbf{V}_{41} + \mathbf{T}_l\mathbf{V}_{41}\mathbf{\Lambda}_1 \\ & - \mathbf{N}\mathbf{V}_{21})\mathbf{\Lambda}_1 - \mathbf{B}\mathbf{Q}_e^{-1}\mathbf{T}_e\mathbf{Q}_e^{-1}\mathbf{K}\mathbf{G}(\mathbf{V}_{41} \\ & + \mathbf{T}_l\mathbf{V}_{41}\mathbf{\Lambda}_1 - \mathbf{N}\mathbf{V}_{21})\mathbf{\Lambda}_1\end{aligned}$$

Then apply equation (30), so that

$$\begin{aligned}\mathbf{V}_{11}\mathbf{\Lambda}_1 - \mathbf{A}\mathbf{V}_{11} \approx\ & \mathbf{B}\mathbf{Q}_e^{-1}\mathbf{K}\mathbf{G}\mathbf{M}\mathbf{V}_{11} \\ & - \mathbf{B}\mathbf{Q}_e^{-1}\mathbf{K}\mathbf{G}\mathbf{T}_l\mathbf{V}_{41}\mathbf{\Lambda}_1 \\ & - \mathbf{B}\mathbf{Q}_e^{-1}\mathbf{K}\mathbf{T}_m\mathbf{Q}_m^{-1}\mathbf{G}\mathbf{M}\mathbf{V}_{11}\mathbf{\Lambda}_1 \\ & - \mathbf{B}\mathbf{Q}_e^{-1}\mathbf{T}_e\mathbf{Q}_e^{-1}\mathbf{K}\mathbf{G}\mathbf{M}\mathbf{V}_{11}\mathbf{\Lambda}_1\end{aligned}$$

Next expand the above expression so that equation (33) is used and

$$\begin{aligned}\mathbf{V}_{11}\mathbf{\Lambda}_1 - \mathbf{A}\mathbf{V}_{11} \approx\ & \mathbf{B}\mathbf{Q}_e^{-1}\mathbf{K}\mathbf{G}\mathbf{M}\mathbf{V}_{11} \\ & - \mathbf{B}\mathbf{Q}_e^{-1}\mathbf{K}\mathbf{G}\mathbf{T}_l\mathbf{Q}_l^{-1}(\mathbf{V}_{41} + \mathbf{T}_l\mathbf{V}_{41}\mathbf{\Lambda}_1)\mathbf{\Lambda}_1 \\ & - \mathbf{B}\mathbf{Q}_e^{-1}\mathbf{K}\mathbf{T}_m\mathbf{Q}_m^{-1}\mathbf{G}\mathbf{M}\mathbf{V}_{11}\mathbf{\Lambda}_1 \\ & - \mathbf{B}\mathbf{Q}_e^{-1}\mathbf{T}_e\mathbf{Q}_e^{-1}\mathbf{K}\mathbf{G}\mathbf{M}\mathbf{V}_{11}\mathbf{\Lambda}_1\end{aligned}$$

or

$$\begin{aligned}\mathbf{V}_{11}\mathbf{\Lambda}_1 - \mathbf{A}\mathbf{V}_{11} \approx\ & \mathbf{B}\mathbf{Q}_e^{-1}\mathbf{K}\mathbf{G}\mathbf{M}\mathbf{V}_{11} \\ & - \mathbf{B}\mathbf{Q}_e^{-1}\mathbf{K}\mathbf{G}\mathbf{T}_l\mathbf{Q}_l^{-1}(\mathbf{M}\mathbf{V}_{11} - \mathbf{N}\mathbf{K}\mathbf{G}\mathbf{V}_{41} \\ & + \mathbf{N}\mathbf{V}_{21})\mathbf{\Lambda}_1 - \mathbf{B}\mathbf{Q}_e^{-1}\mathbf{K}\mathbf{T}_m\mathbf{Q}_m^{-1}\mathbf{G}\mathbf{M}\mathbf{V}_{11}\mathbf{\Lambda}_1 \\ & - \mathbf{B}\mathbf{Q}_e^{-1}\mathbf{T}_e\mathbf{Q}_e^{-1}\mathbf{K}\mathbf{G}\mathbf{M}\mathbf{V}_{11}\mathbf{\Lambda}_1\end{aligned}$$

Equations (29) and (28) are subsequently applied to eliminate the last $\mathbf{V}_{41}$ term; thus,

$$\begin{aligned}\mathbf{V}_{11}\mathbf{\Lambda}_1 - \mathbf{A}\mathbf{V}_{11} \approx\ & \mathbf{B}\mathbf{Q}_e^{-1}\mathbf{K}\mathbf{G}\mathbf{M}\mathbf{V}_{11} \\ & - \mathbf{B}\mathbf{Q}_e^{-1}\mathbf{K}\mathbf{G}\mathbf{T}_l\mathbf{Q}_l^{-1}(\mathbf{M}\mathbf{V}_{11} - \mathbf{N}\mathbf{V}_{21} \\ & + \mathbf{N}\mathbf{V}_{21})\mathbf{\Lambda}_1 - \mathbf{B}\mathbf{Q}_e^{-1}\mathbf{K}\mathbf{T}_m\mathbf{Q}_m^{-1}\mathbf{G}\mathbf{M}\mathbf{V}_{11}\mathbf{\Lambda}_1 \\ & - \mathbf{B}\mathbf{Q}_e^{-1}\mathbf{T}_e\mathbf{Q}_e^{-1}\mathbf{K}\mathbf{G}\mathbf{M}\mathbf{V}_{11}\mathbf{\Lambda}_1\end{aligned}$$

All unwanted terms are eliminated, so that

$$\begin{aligned}\mathbf{V}_{11}\mathbf{\Lambda}_1 - \mathbf{A}\mathbf{V}_{11} \approx\ & \mathbf{B}\mathbf{Q}_e^{-1}\mathbf{K}\mathbf{G}\mathbf{M}\mathbf{V}_{11} \\ & - \mathbf{B}\mathbf{Q}_e^{-1}\mathbf{K}\mathbf{G}\mathbf{T}_l\mathbf{Q}_l^{-1}\mathbf{M}\mathbf{V}_{11}\mathbf{\Lambda}_1 \\ & - \mathbf{B}\mathbf{Q}_e^{-1}\mathbf{K}\mathbf{T}_m\mathbf{Q}_m^{-1}\mathbf{G}\mathbf{M}\mathbf{V}_{11}\mathbf{\Lambda}_1 \\ & - \mathbf{B}\mathbf{Q}_e^{-1}\mathbf{T}_e\mathbf{Q}_e^{-1}\mathbf{K}\mathbf{G}\mathbf{M}\mathbf{V}_{11}\mathbf{\Lambda}_1\end{aligned}$$

Finally, note that

$$\mathbf{Q}_e^{-1}\mathbf{K}\mathbf{G} = (\mathbf{I} - \mathbf{K}\mathbf{G}\mathbf{N})^{-1}\mathbf{K}\mathbf{G} = \mathbf{K}\mathbf{G}(\mathbf{I} - \mathbf{N}\mathbf{K}\mathbf{G})^{-1} = \mathbf{K}\mathbf{G}\mathbf{Q}_l^{-1}$$

$$\mathbf{Q}_e^{-1}\mathbf{K} = (\mathbf{I} - \mathbf{K}\mathbf{G}\mathbf{N})^{-1}\mathbf{K} = \mathbf{K}(\mathbf{I} - \mathbf{G}\mathbf{N}\mathbf{K})^{-1} = \mathbf{K}\mathbf{Q}_m^{-1}$$

by the matrix inversion lemma. The approximation is then converted to the familiar form:

$$\begin{aligned}\mathbf{V}_{11}\mathbf{\Lambda}_1 - \mathbf{A}\mathbf{V}_{11} \approx\ & \mathbf{B}\mathbf{Q}_e^{-1}\mathbf{K}\mathbf{G}\mathbf{M}\mathbf{V}_{11} \\ & - \mathbf{B}\mathbf{K}\mathbf{G}\mathbf{Q}_l^{-1}\mathbf{T}_l\mathbf{Q}_l^{-1}\mathbf{M}\mathbf{V}_{11}\mathbf{\Lambda}_1 \\ & - \mathbf{B}\mathbf{K}\mathbf{Q}_m^{-1}\mathbf{T}_m\mathbf{Q}_m^{-1}\mathbf{G}\mathbf{M}\mathbf{V}_{11}\mathbf{\Lambda}_1 \\ & - \mathbf{B}\mathbf{Q}_e^{-1}\mathbf{T}_e\mathbf{Q}_e^{-1}\mathbf{K}\mathbf{G}\mathbf{M}\mathbf{V}_{11}\mathbf{\Lambda}_1\end{aligned}$$

Postmultiplying the result by $\mathbf{V}_{11}^{-1}$ yields

$$\begin{aligned}\mathbf{A}_{LO} \approx\ & (\mathbf{A}_{FO})_{rb} + \mathbf{B}\mathbf{K}\mathbf{G}\mathbf{Q}_l^{-1}\mathbf{T}_l\mathbf{Q}_l^{-1}\mathbf{M}(\mathbf{A}_{FO})_{rb} \\ & + \mathbf{B}\mathbf{K}\mathbf{Q}_m^{-1}\mathbf{T}_m\mathbf{Q}_m^{-1}\mathbf{G}\mathbf{M}(\mathbf{A}_{FO})_{rb} \\ & + \mathbf{B}\mathbf{Q}_e^{-1}\mathbf{T}_e\mathbf{Q}_e^{-1}\mathbf{K}\mathbf{G}\mathbf{M}(\mathbf{A}_{FO})_{rb}\end{aligned}$$

where

$$\mathbf{A}_{LO} = \mathbf{A} + \mathbf{B}\mathbf{Q}_e^{-1}\mathbf{K}\mathbf{G}\mathbf{M}$$

$$(\mathbf{A}_{FO})_{rb} = \mathbf{V}_{11}\mathbf{\Lambda}_1\mathbf{V}_{11}^{-1}$$

The eigenspace transformation matrix is now

$$\begin{aligned}\mathbf{E} = \mathbf{I} + \mathbf{B}\mathbf{K}\mathbf{G}\mathbf{Q}_l^{-1}\mathbf{T}_l\mathbf{Q}_l^{-1}\mathbf{M} + \mathbf{B}\mathbf{K}\mathbf{Q}_m^{-1}\mathbf{T}_m\mathbf{Q}_m^{-1}\mathbf{G}\mathbf{M} \\ + \mathbf{B}\mathbf{Q}_e^{-1}\mathbf{T}_e\mathbf{Q}_e^{-1}\mathbf{K}\mathbf{G}\mathbf{M}\end{aligned} \tag{34}$$

Note that the previous derivation for first-order lag actuator models is a subset of this result. If the first-order lag at any one of these points is not present, then the associated time constant is 0. In addition, within each matrix of time constants, any of the elements can be 0 when that particular signal does not have a lag to be modeled.

Two or more first-order lags in series at a particular location in the system are handled in a simple way. The time constants associated with each channel only need to be summed before applying equation (34). For example, the approximate eigenspace transformation matrix of two first-order lags in series with time constants of 0.01 sec and 0.02 sec

$$\begin{aligned}\left(\frac{1}{0.01s+1}\right)\left(\frac{1}{0.02s+1}\right) &= \frac{1}{0.002s^2+0.03s+1} \\ &\approx \frac{1}{0.03s+1}\end{aligned}$$

will be the same as that of a single first-order lag with a time constant of 0.03 sec. Note that this substitution will be good over the frequency range of the rigid-body dynamics.

Application

By using the subset of equation (34) that corresponds to a system with first-order lag in controls, one obtains

$$\mathbf{E} = \mathbf{I} + \mathbf{B}\mathbf{K}\mathbf{Q}_m^{-1}\mathbf{T}_m\mathbf{Q}_m^{-1}\mathbf{G}\mathbf{M} \tag{35}$$

where

$$\mathbf{Q}_m \equiv \mathbf{I} - \mathbf{G}\mathbf{N}\mathbf{K}$$

$$\mathbf{A}_{LO} = \mathbf{A} + \mathbf{B}\mathbf{Q}_e^{-1}\mathbf{K}\mathbf{G}\mathbf{M}$$

These results will be used to predict the effect of the roll-off filters shown in figure 4. The roll-off filter transfer function is

$$TF_{RO}(s) = \frac{1}{\frac{1}{25}s+1}$$

in each channel. Therefore, for this example, the eigenspace transformation matrix is

$$\mathbf{E} = \mathbf{I} + \mathbf{B}\mathbf{K}\mathbf{Q}_m^{-1}\begin{bmatrix}\frac{1}{25} & 0 \\ 0 & \frac{1}{25}\end{bmatrix}\mathbf{Q}_m^{-1}\mathbf{G}\mathbf{M} \tag{36}$$

The purpose of the roll-off filter is to attenuate high-frequency commands. This attenuation should reduce potential problems caused by structural dynamics or noise. Results similar to those of the actuators are expected, since both the actuators and the roll-off filters are first-order lags. Figure 15 shows the predicted effect of the filters on the roll mode pole. The predicted effect of the filters on the Dutch roll mode pole is shown in figure 16. Figure 17 shows the predicted effect of the filters on modal coupling. The effect of these unmodeled dynamics is more pronounced because the roll-off filters are slower than the actuators. Again, the approximate eigenspace transformation matrix accurately predicts the rigid-body eigenspace of this full-order, closed-loop system.

Higher-Order Filters

Equivalent First-Order Lag

Now that the eigenspace transformation is available to predict the effects that first-order lags have on the rigid-body eigenspace of the full-order, closed-loop system, it is useful to generalize the transformation to higher order filters. More specifically, one would like to handle dynamics such as lead or lag compensators, transport delays, and notch filters. Handling these dynamics is essential when faced with the second-order filters found in the HARV flight control system. A system with unmodeled higher order filters on the controls is shown in figure 18. The feedthrough term has been removed for this analysis.

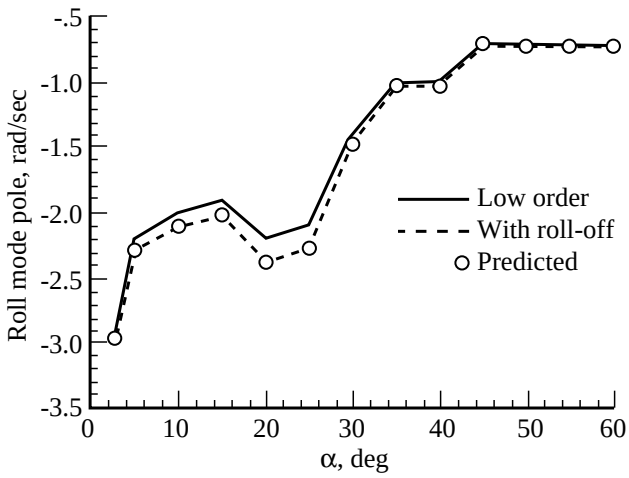

Figure 15. Roll mode pole prediction with roll-off filters.

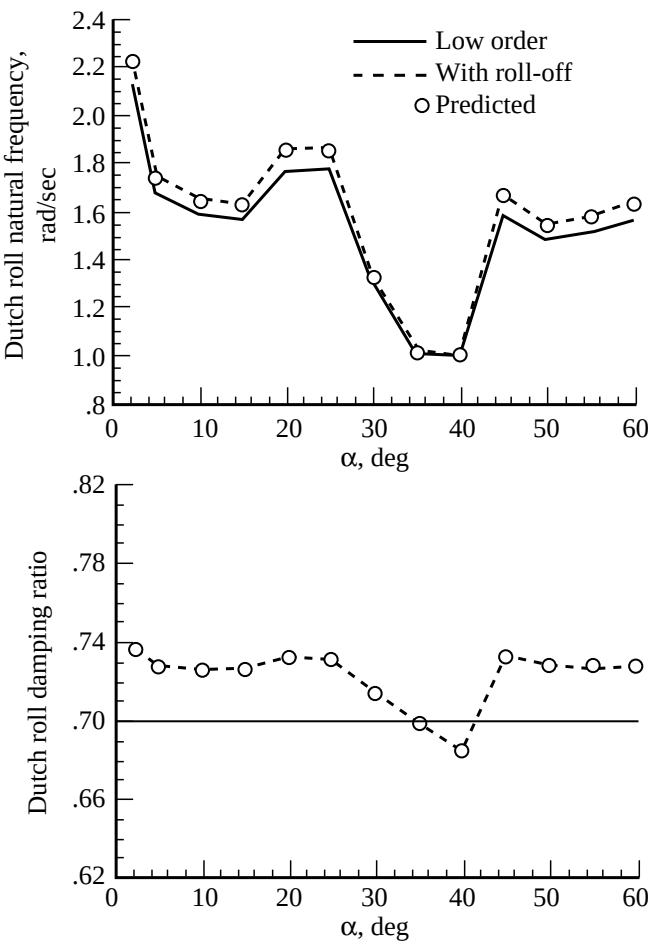

Figure 16. Dutch roll mode pole prediction with roll-off filters.

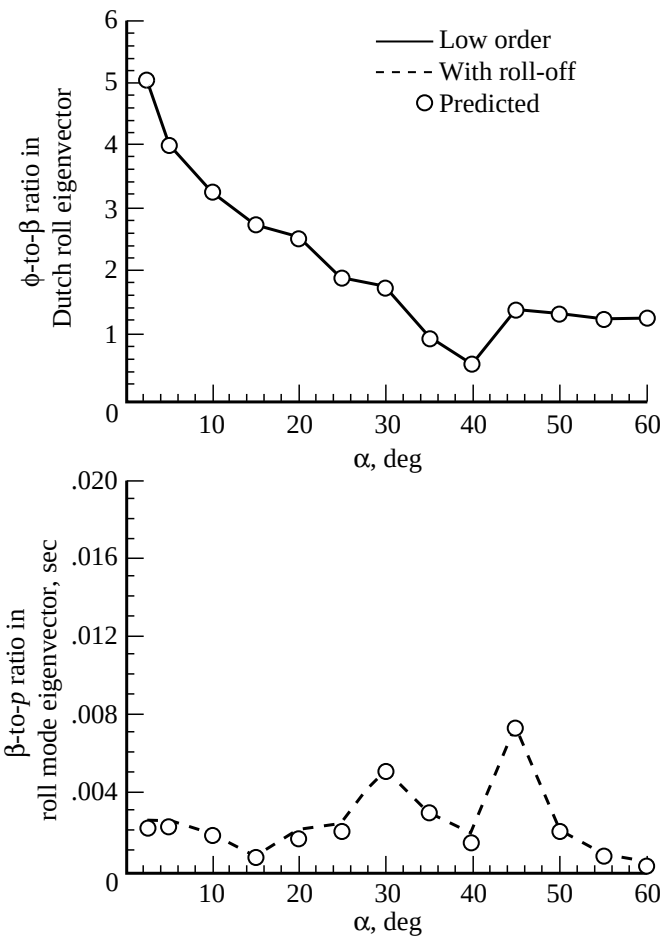

Figure 17. Eigenvector prediction with roll-off filters.

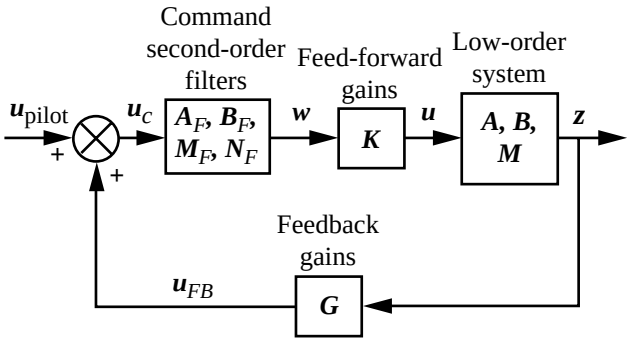

Figure 18. System block diagram with second-order command filters as unmodeled dynamics.

The system can be written as follows:

$$\dot{\mathbf{x}} = \mathbf{A}\mathbf{x} + \mathbf{B}\mathbf{K}\mathbf{w} \qquad \text{(System dynamics/ feed-forward gains)}$$

$$\mathbf{z} = \mathbf{M}\mathbf{x} \qquad \text{(System measurements)}$$

$$\mathbf{u}_{FB} = \mathbf{G}\mathbf{z} \qquad \text{(Feedback control)}$$

$$\mathbf{u}_c = \mathbf{u}_{FB} + \mathbf{u}_{\text{pilot}} \qquad \text{(Feed-forward control)}$$

$$\dot{\mathbf{v}} = \mathbf{A}_F\mathbf{v} + \mathbf{B}_F\mathbf{u}_c \qquad \text{(Filter system dynamics)}$$

$$\mathbf{w} = \mathbf{M}_F\mathbf{v} + \mathbf{N}_F\mathbf{u}_c \qquad \text{(Filter measurements)}$$

where the filters in parallel channels are realized as

$$\mathbf{A}_F = \begin{bmatrix} \mathbf{A}_{f_1} & & 0 \\ & \ddots & \\ 0 & & \mathbf{A}_{f_m} \end{bmatrix}$$

$$\mathbf{B}_F = \begin{bmatrix} \mathbf{B}_{f_1} & & 0 \\ & \ddots & \\ 0 & & \mathbf{B}_{f_m} \end{bmatrix}$$

$$\mathbf{M}_F = \begin{bmatrix} \mathbf{M}_{f_1} & & 0 \\ & \ddots & \\ 0 & & \mathbf{M}_{f_m} \end{bmatrix}$$

$$\mathbf{N}_F = \begin{bmatrix} \mathbf{N}_{f_1} & & 0 \\ & \ddots & \\ 0 & & \mathbf{N}_{f_m} \end{bmatrix}$$

thus giving each higher order filter a transfer function of the form

$$\mathbf{M}_{f_i}\left(s\mathbf{I} - \mathbf{A}_{f_i}\right)^{-1}\mathbf{B}_{f_i} + \mathbf{N}_{f_i} \qquad (i = 1, 2, \ldots, m)$$

The closed-loop system matrix spectral decomposition for this system is

$$\begin{bmatrix} \mathbf{A} + \mathbf{B}\mathbf{K}\mathbf{N}_F\mathbf{G}\mathbf{M} & \mathbf{B}\mathbf{K}\mathbf{M}_F \\ \mathbf{B}_F\mathbf{G}\mathbf{M} & \mathbf{A}_F \end{bmatrix} \begin{bmatrix} \mathbf{V}_{11} & \mathbf{V}_{12} \\ \mathbf{V}_{21} & \mathbf{V}_{22} \end{bmatrix}$$

$$= \begin{bmatrix} \mathbf{V}_{11} & \mathbf{V}_{12} \\ \mathbf{V}_{21} & \mathbf{V}_{22} \end{bmatrix} \begin{bmatrix} \mathbf{\Lambda}_1 & 0 \\ 0 & \mathbf{\Lambda}_2 \end{bmatrix}$$

where again $\mathbf{\Lambda}_1$ and $\mathbf{V}_{11}$ correspond to the rigid-body eigenspace. When multiplied out, this equation yields four matrix equations. Two of these equations, which correspond to the upper left and lower left partitions, can be written as

$$\mathbf{V}_{11}\mathbf{\Lambda}_1 - (\mathbf{A} + \mathbf{B}\mathbf{K}\mathbf{N}_F\mathbf{G}\mathbf{M})\mathbf{V}_{11} = \mathbf{B}\mathbf{K}\mathbf{M}_F\mathbf{V}_{21} \quad (37)$$

$$-\mathbf{A}_F^{-1}\mathbf{B}_F\mathbf{G}\mathbf{M}\mathbf{V}_{11} = \mathbf{V}_{21} - \mathbf{A}_F^{-1}\mathbf{V}_{21}\mathbf{\Lambda}_1 \quad (38)$$

where it is assumed that the higher order filters have no poles at the origin. Equation (37) is expanded by methods used in previous sections to yield the infinite series

$$\begin{aligned} &\mathbf{V}_{11}\mathbf{\Lambda}_1 - \mathbf{A}\mathbf{V}_{11} - \mathbf{B}\mathbf{K}\mathbf{N}_F\mathbf{G}\mathbf{M}\mathbf{V}_{11} \\ &\quad = \mathbf{B}\mathbf{K}\mathbf{M}_F(\mathbf{V}_{21} - \mathbf{A}_F^{-1}\mathbf{V}_{21}\mathbf{\Lambda}_1) + \mathbf{B}\mathbf{K}\mathbf{M}_F\mathbf{A}_F^{-1}(\mathbf{V}_{21} \\ &\qquad - \mathbf{A}_F^{-1}\mathbf{V}_{21}\mathbf{\Lambda}_1)\mathbf{\Lambda}_1 + \mathbf{B}\mathbf{K}\mathbf{M}_F\mathbf{A}_F^{-2}(\mathbf{V}_{21} - \mathbf{A}_F^{-1}\mathbf{V}_{21}\mathbf{\Lambda}_1)\mathbf{\Lambda}_1^2 + \ldots \end{aligned}$$

Substituting equation (38) yields

$$\begin{aligned} &\mathbf{V}_{11}\mathbf{\Lambda}_1 - \mathbf{A}\mathbf{V}_{11} - \mathbf{B}\mathbf{K}\mathbf{N}_F\mathbf{G}\mathbf{M}\mathbf{V}_{11} \\ &\quad = -\mathbf{B}\mathbf{K}\mathbf{M}_F\mathbf{A}_F^{-1}\mathbf{B}_F\mathbf{G}\mathbf{M}\mathbf{V}_{11} \\ &\qquad - \mathbf{B}\mathbf{K}\mathbf{M}_F\mathbf{A}_F^{-2}\mathbf{B}_F\mathbf{G}\mathbf{M}\mathbf{V}_{11}\mathbf{\Lambda}_1 - \mathbf{B}\mathbf{K}\mathbf{M}_F\mathbf{A}_F^{-3}\mathbf{G}\mathbf{M}\mathbf{V}_{11}\mathbf{\Lambda}_1^2 - \ldots \end{aligned}$$

Postmultiplying by $\mathbf{V}_{11}^{-1}$, we get

$$\begin{aligned} (\mathbf{A}_{FO})_{rb} = \mathbf{A} &+ \mathbf{B}\mathbf{K}\mathbf{N}_F\mathbf{G}\mathbf{M} - \mathbf{B}\mathbf{K}\mathbf{M}_F\mathbf{A}_F^{-1}\mathbf{B}_F\mathbf{G}\mathbf{M} \\ &- \mathbf{B}\mathbf{K}\mathbf{M}_F\mathbf{A}_F^{-2}\mathbf{B}_F\mathbf{G}\mathbf{M}(\mathbf{A}_{FO})_{rb} \\ &- \mathbf{B}\mathbf{K}\mathbf{M}_F\mathbf{A}_F^{-3}\mathbf{B}_F\mathbf{G}\mathbf{M}(\mathbf{A}_{FO})_{rb}^2 - \ldots \end{aligned} \quad (39)$$

The type of higher order filters considered is restricted to those with a steady-state gain of 1 through all channels. The steady-state gain is the limit of the filter transfer function as s goes to 0. This gain of 1 yields the relations

$$-\mathbf{M}_{f_i}\mathbf{A}_{f_i}^{-1}\mathbf{B}_{f_i} + \mathbf{N}_{f_i} = 1$$

or

$$-\mathbf{M}_F\mathbf{A}_F^{-1}\mathbf{B}_F + \mathbf{N}_F = \mathbf{I}$$

Using this result to combine the first three terms on the right-hand side of equation (39), we get

$$\begin{aligned} \mathbf{A}_{LO} = (\mathbf{A}_{FO})_{rb} &+ \mathbf{B}\mathbf{K}\mathbf{M}_F\mathbf{A}_F^{-2}\mathbf{B}_F\mathbf{G}\mathbf{M}(\mathbf{A}_{FO})_{rb} \\ &+ \mathbf{B}\mathbf{K}\mathbf{M}_F\mathbf{A}_F^{-3}\mathbf{B}_F\mathbf{G}\mathbf{M}(\mathbf{A}_{FO})_{rb}^2 + \ldots \end{aligned} \quad (40)$$

The approximate eigenspace transformation matrix of any higher order filter with a steady-state gain of 1 is the same as that of a first-order lag with an equivalent time constant matrix equal to $\mathbf{M}_F\mathbf{A}_F^{-2}\mathbf{B}_F$.

Second-order filter. A second-order filter modeled as the transfer function

$$\frac{w_i(s)}{u_i(s)} = \frac{\omega_{\text{den}_i}^2}{\omega_{\text{num}_i}^2}\left(\frac{s^2 + 2\zeta_{\text{num}_i}\omega_{\text{num}_i}s + \omega_{\text{num}_i}^2}{s^2 + 2\zeta_{\text{den}_i}\omega_{\text{den}_i}s + \omega_{\text{den}_i}^2}\right)$$

has the following system matrices

$$\mathbf{A}_{f_i} = \begin{bmatrix} 0 & -\omega_{\text{den}_i}^2 \\ 1 & -2\zeta_{\text{den}_i}\omega_{\text{den}_i} \end{bmatrix} \qquad (i = 1, 2, \ldots, m)$$

$$\mathbf{B}_{f_i} = \frac{\omega_{\text{den}_i}^2}{\omega_{\text{num}_i}^2} \begin{bmatrix} \omega_{\text{num}_i}^2 - \omega_{\text{den}_i}^2 \\ 2\left(\zeta_{\text{num}_i}\omega_{\text{num}_i} - \zeta_{\text{den}_i}\omega_{\text{den}_i}\right) \end{bmatrix}$$

$$\mathbf{M}_{f_i} = [0 \quad 1]$$

$$\mathbf{N}_{f_i} = \frac{\omega_{\text{den}_i}^2}{\omega_{\text{num}_i}^2}$$

The equivalent time constant is $\mathbf{M}_{f_i}\mathbf{A}_{f_i}^{-2}\mathbf{B}_{f_i}$ or

$$\tau_i = 2\left(\frac{\zeta_{\text{den}_i}}{\omega_{\text{den}_i}} - \frac{\zeta_{\text{num}_i}}{\omega_{\text{num}_i}}\right) \tag{41}$$

As an example, consider a notch filter with a denominator damping ratio of 0.7, a numerator damping ratio of 0.1, and equal natural frequencies in the numerator and the denominator. From equation (41), we see that the effect of the filter on the rigid-body eigenspace will be virtually the same as that of a first-order lag with a break frequency of 83 percent of the natural frequency of the notch filter.

Time delay. The first-order Padé approximation to a transport delay is written as

$$\frac{w_i(s)}{u_i(s)} = \frac{1 - (t_{d_i}/2)\, s}{1 + (t_{d_i}/2)\, s}$$

The system matrices can be written as

$$\mathbf{A}_{f_i} = \frac{-2}{t_{d_i}} \qquad \mathbf{B}_{f_i} = \frac{4}{t_{d_i}}$$

$$\mathbf{M}_{f_i} = 1 \qquad \mathbf{N}_{f_i} = -1$$

The appropriate first-order lag for this transfer function is found to have a time constant equal to the transport delay magnitude such that

$$\tau_i = t_{d_i}$$

Lead/lag compensator. Another type of filter that has been considered is a lead/lag compensator of the form

$$\frac{w_i(s)}{u_i(s)} = \frac{\tau_{\text{num}_i} s + 1}{\tau_{\text{den}_i} s + 1}$$

or in state-space form

$$\mathbf{A}_{f_i} = \frac{-1}{\tau_{\text{den}_i}} \qquad \mathbf{B}_{f_i} = \frac{\tau_{\text{den}_i} - \tau_{\text{num}_i}}{\tau_{\text{den}_i}^2}$$

$$\mathbf{M}_{f_i} = 1 \qquad \mathbf{N}_{f_i} = \frac{\tau_{\text{num}_i}}{\tau_{\text{den}_i}}$$

The rigid-body eigenspace of the full-order, closed-loop system that includes this filter can be accurately predicted using the eigenspace transformation matrix corresponding to a first-order lag with a time constant of

$$\tau_i = \tau_{\text{den}_i} - \tau_{\text{num}_i}$$

This result implies that such a compensator could be designed to cancel much of the effect of unmodeled dynamics on the rigid-body eigenspace.

Application

The HARV lateral-directional second-order filters have the transfer function

$$TF(s) = \frac{\omega_{\text{den}}^2}{\omega_{\text{num}}^2}\left(\frac{s^2 + 2\zeta_{\text{num}}\omega_{\text{num}}s + \omega_{\text{num}}^2}{s^2 + 2\zeta_{\text{den}}\omega_{\text{den}}s + \omega_{\text{den}}^2}\right)$$

with characteristics shown in table 1. The first two characteristics listed are the command filters; the remaining five are measurement notch filters. The two lateral acceleration filters are configured in series. Each of these two filter sets will now be considered.

Table 1. HARV Second-Order Filters

Filtered signals	ω_{den}, rad/sec	ζ_{den}	ω_{num}, rad/sec	ζ_{num}
$\dot{p}_c$	40	0.6	140	0.74
$\dot{r}_c$	40	.6	140	.74
p_b	80	.7	80	.08
r_b	150	.7	150	.08
$n_{y_{\text{sens}}}$	58	.7	58	.08
	80	.7	80	.08
$\dot{\beta}_{\text{sens}}$	80	.7	80	.10

For the command filters, equations (34) and (41) imply that the eigenspace transformation matrix should be

$$\mathbf{E} = \mathbf{I} + \mathbf{BKQ}_m^{-1} \begin{bmatrix} 0.0194 & 0 \\ 0 & 0.0194 \end{bmatrix} \mathbf{Q}_m^{-1}\mathbf{GM} \tag{42}$$

Although a feed-through term was not included when deriving the equivalent time constants for higher order filters, it has been postulated that the feed-through term should be handled in the same way as suggested in previous sections.

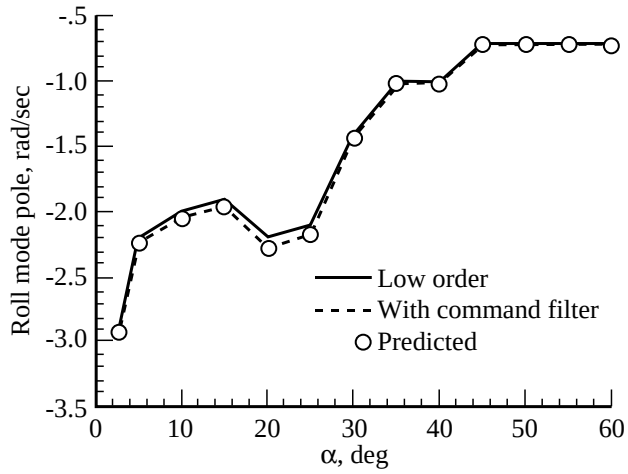

Figure 19. Roll mode pole prediction with command second-order filters.

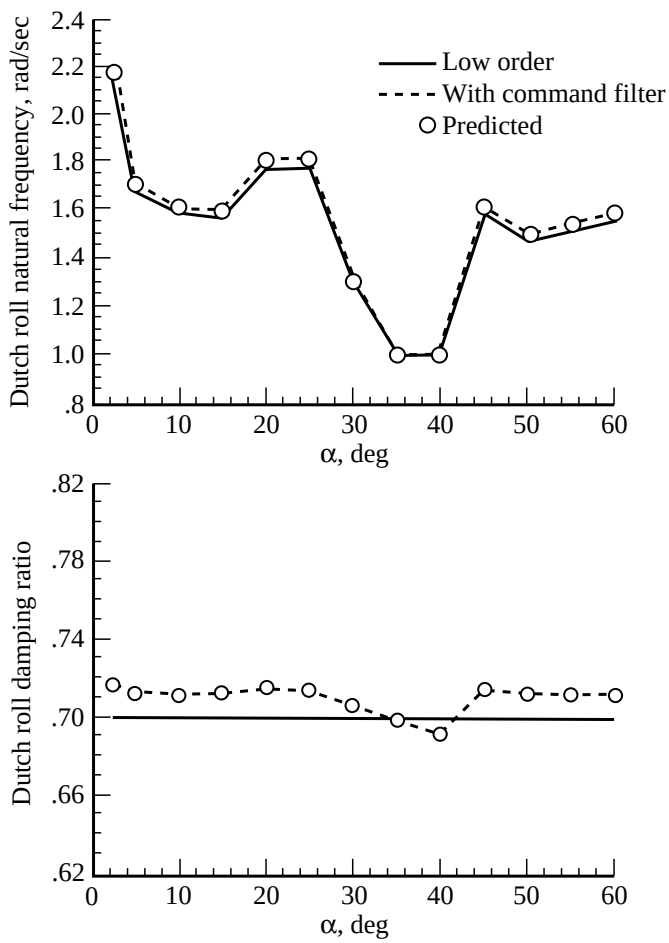

Figure 20. Dutch roll mode pole prediction with command second-order filters.

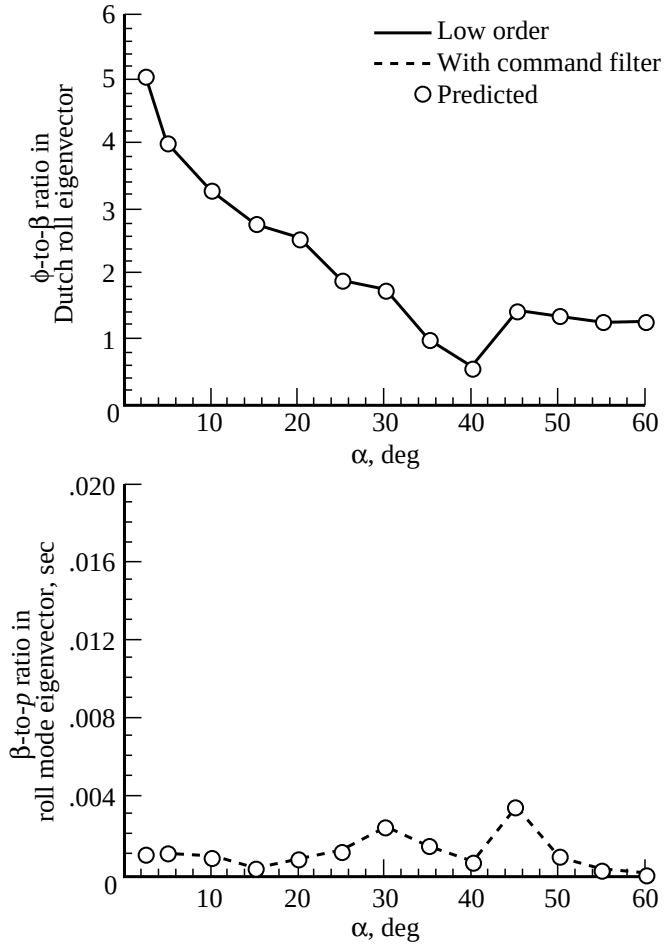

Figure 21. Eigenvector prediction with command second-order filters.

From the previous discussion, these second-order command filters, having zeros with frequencies of 140 rad/sec and poles with frequencies of 40 rad/sec, will affect the rigid-body eigenspace of the full-order, closed-loop system in the same manner as a roll-off filter with a time constant of 0.0194 sec. The eigenspace results are shown in figures 19, 20, and 21. Again, the approximate eigenspace transformation matrix accurately predicts the resulting rigid-body eigenspace.

The second-order filters in the measurement loop are notch filters designed to cancel resonant peaks in the structural model. There are two second-order filters in series for the $n_{y_{\text{sens}}}$ channel, so the approximate time constant associated with each will be summed to approximate the effect of both. The eigenspace transformation matrix associated with the

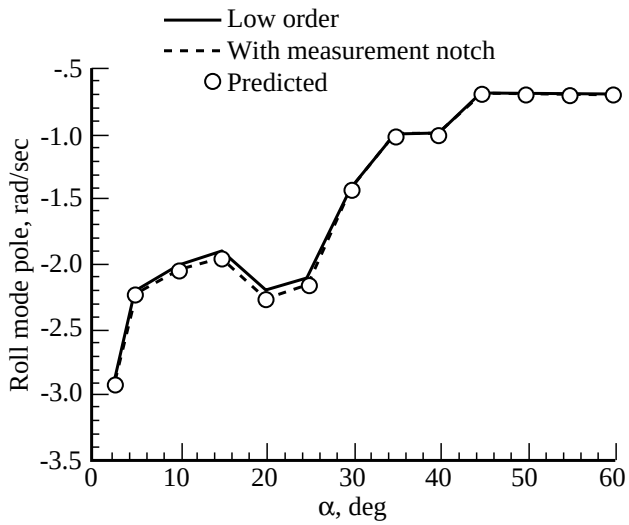

Figure 22. Roll mode pole prediction with measurement notch filters.

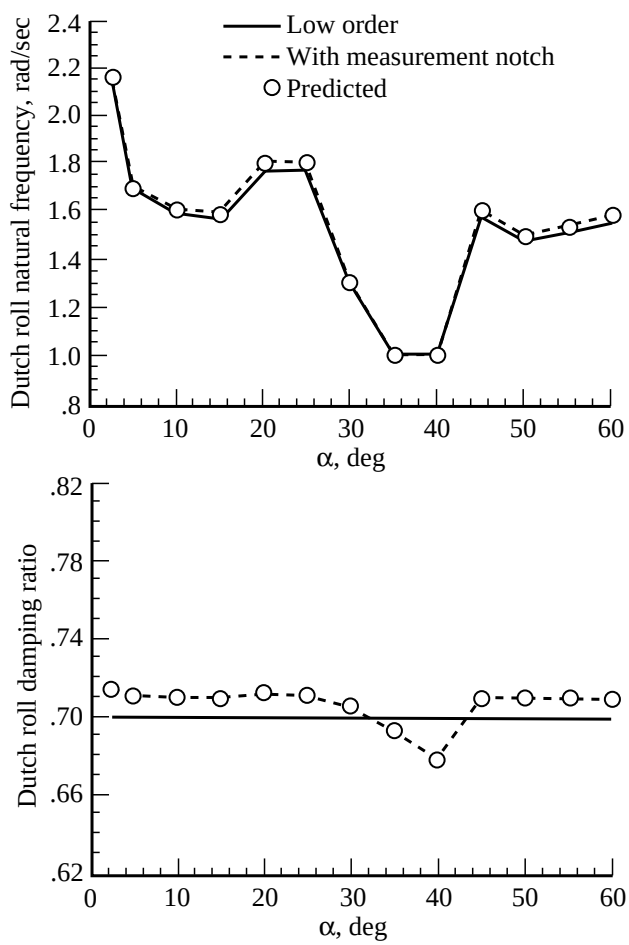

Figure 23. Dutch roll mode pole prediction with measurement notch filters.

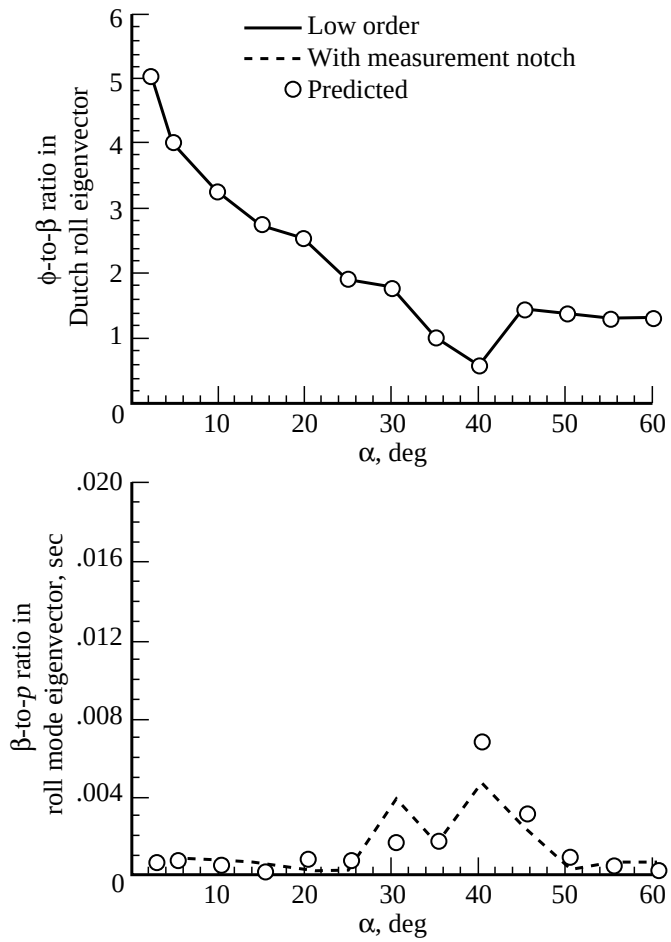

Figure 24. Eigenvector prediction with measurement notch filters.

measurement notch filters is, from equations (34) and (41),

$$\mathbf{E} = \mathbf{I} + \mathbf{BKGQ}_l^{-1} \begin{bmatrix} 0.0155 & & & 0 \\ & 0.0083 & & \\ & & 0.0369 & \\ 0 & & & 0.0150 \end{bmatrix} \mathbf{Q}_l^{-1}\mathbf{M} \tag{43}$$

The effects of these notch filters are shown in figures 22, 23, and 24. The eigenvalues and eigenvectors of $\mathbf{E}^{-1}\mathbf{A}_{LO}$ predict very well the resulting rigid-body eigenspace. Only a slight degradation in the prediction of the small β-to-p ratio in the roll mode effect is observed. Hence, the approximate first-order lags are a suitable substitute for the higher order filters in this example.

This section has shown how the effects of higher order filters on the closed-loop rigid-body eigenspace can be evaluated using first-order lags placed at the same loop location. This result is expected as long as

the steady-state gains of the unmodeled higher order filters are unity.

HARV Full-Order, Closed-Loop System

An approach is now proposed to predict the simultaneous effect of all unmodeled dynamics (which is introduced in the section entitled "Full-Order, Closed-Loop System") on the HARV control law design. The strategy is straightforward: approximate the HARV full-order, closed-loop system of figure 4 using the closed-loop system in figure 14 by replacing all unmodeled dynamics with equivalent first-order lag components. Equation (34), which defines the eigenspace transformation matrix in this simpler case, is then directly applied.

The full-order, closed-loop system is placed in the simpler form as follows. Note that the actuators are already modeled by first-order lags; therefore, nothing needs to be done. Turning to the other unmodeled dynamics, the second-order command and measurement notch filters are replaced by approximate first-order lags derived in the section entitled "Higher Order Filters." Here, it is postulated that the results of that section, which were only considered filters at a single-loop location, extend to filters at multiple-loop locations. Next, the filters in series (i.e., the first-order roll-off and approximate command filters) are replaced by single first-order lags. The time constant of the approximate lag equals the sum of the time constants of the replaced lags; this leads to a system of the form shown in figure 14 with first-order lag elements at three separate loop locations. Equation (34) can then be used to obtain the eigenspace transformation matrix, where (from eq. (25)),

$$\mathbf{T}_e = \begin{bmatrix} 0.0208 & & & & 0 \\ & 0.0250 & & & \\ & & 0.0333 & & \\ & & & 0.0208 & \\ 0 & & & & 0.0208 \end{bmatrix}$$

From equations (36) and (42),

$$\mathbf{T}_m = \begin{bmatrix} 0.04 & 0 \\ 0 & 0.04 \end{bmatrix} + \begin{bmatrix} 0.0194 & 0 \\ 0 & 0.0194 \end{bmatrix} = \begin{bmatrix} 0.0594 & 0 \\ 0 & 0.0594 \end{bmatrix}$$

From equation (43),

$$\mathbf{T}_l = \begin{bmatrix} 0.0155 & & & 0 \\ & 0.0083 & & \\ & & 0.0369 & \\ 0 & & & 0.0150 \end{bmatrix}$$

Figure 25 shows the prediction of the roll mode pole. Figure 26 shows the Dutch roll mode pole.

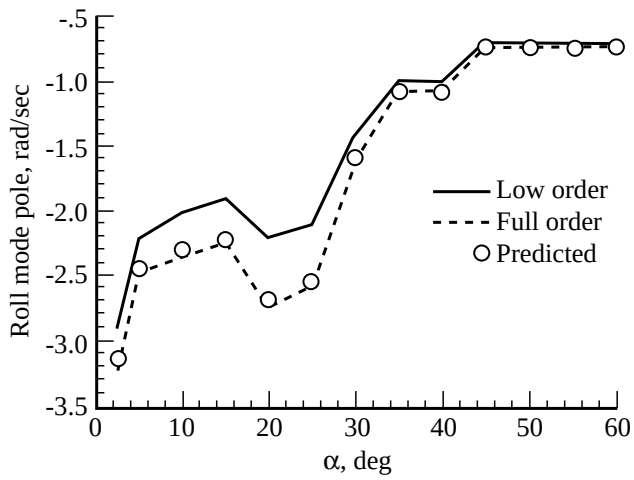

Figure 25. Roll mode pole prediction with full-order model.

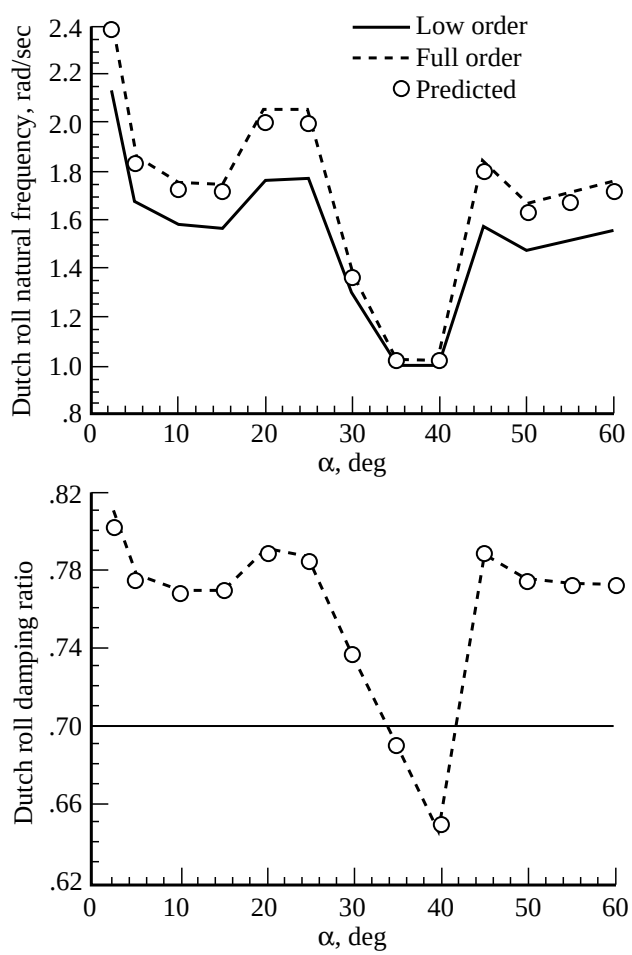

Figure 26. Dutch roll mode pole prediction with full-order model.

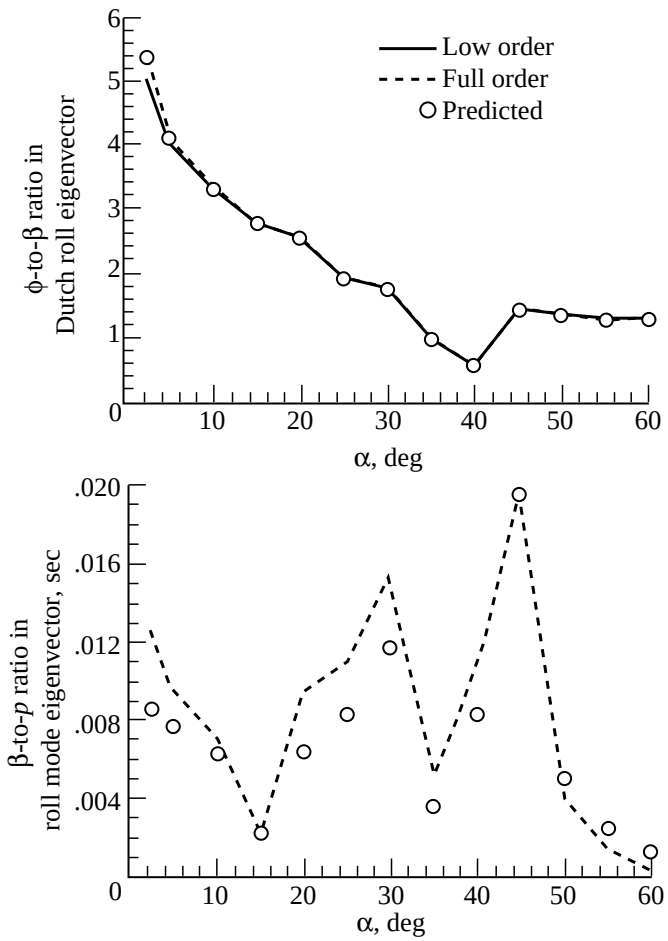

Figure 27. Eigenvector prediction with full-order model.

Figure 27 contains the eigenvector element ratio prediction. As before, the eigenvalues and the eigenvectors of $\mathbf{E}^{-1}\mathbf{A}_{LO}$ predict the rigid-body eigenspace of the 25th-order, closed-loop system.

Conclusions and Recommendations

The approach presented in this report allows the control law designer to predict to what extent unmodeled dynamics affect the closed-loop, rigid-body eigenspace. Such insight is important when deciding which dynamics will be included in the model used to design the controller. A single-input, single-output example was used to illustrate and predict the effect of unmodeled dynamics on a closed-loop, rigid-body pole. This result was extended to multiple-input, multiple-output dynamics, thus leading to the concept of an eigenspace transformation matrix that relates the desired closed-loop rigid-body eigenspace to that obtained in the presence of unmodeled dynamics.

The approach was first developed for unmodeled first-order lag elements at one specific loop location and then extended to multiple-loop locations. The eigenspace transformation matrix was shown to accurately predict the achieved rigid-body eigenspace for this type of unmodeled dynamics. For higher order unmodeled filters with a steady-state gain of unity, derived approximate first-order lag components were shown to be a suitable replacement in predicting the achieved rigid-body eigenspace. The approximate components were easily found from the state-space expressions of the unmodeled higher order filters. Also, the aggregate effect of many types of unmodeled dynamics on the achieved rigid-body eigenspace was shown to be well predicted.

In conclusion, note that there will always be some errors in the achieved rigid-body eigenspace, whether they are caused by poor mathematical models, off-design flight conditions, or unmodeled dynamics. The goal is to find what these errors are and determine if they will be acceptable. A method for predicting how some unmodeled dynamics affect the rigid-body eigenspace is now available.

Some important areas of future work suggested by this research include the following:

1. Developing a method to predict the achieved rigid-body dynamics when a significant frequency separation does not exist between the rigid-body and unmodeled dynamics (i.e., when the convergence criteria would be violated)

2. Formulating sensitivity relationships that determine changes in the achieved rigid-body dynamics caused by incremental changes in unmodeled equivalent first-order lag time constants

3. Developing a desired eigenspace adjustment procedure to account for the effect of unmodeled dynamics on the final full-order, closed-loop eigenspace using the eigenspace transformation matrix concept

4. Developing methods to change the design model, instead of the desired eigenspace, to account for the effect of unmodeled dynamics in the control system design process

NASA Langley Research Center
Hampton, VA 23681-0001
January 31, 1994

Appendix A

HARV Lateral-Directional Aircraft Model

This appendix contains the linear models representing the High Alpha Research Vehicle (HARV) lateral-directional rigid-body aircraft dynamics at the 13 flight conditions used in this study. A full nonlinear model (ref. 7), written in the Advanced Control Simulation Language (ACSL), was used to generate these Jacobians. The form of the linear system is

$$\dot{\mathbf{x}} = \mathbf{A}\mathbf{x} + \mathbf{B}\mathbf{u} \qquad \text{(Low-order dynamics)}$$

$$\mathbf{z} = \mathbf{M}\mathbf{x} + \mathbf{N}\mathbf{u} \qquad \text{(System measurements)}$$

with four states, four measurements, and five effectors. The states are lateral velocity, stability-axis roll rate, stability-axis yaw rate, and bank angle (given in units of feet per second, radians per second, radians per second, and radians, respectively). The measurements are body-axis roll rate, body-axis yaw rate, lateral acceleration, and sideslip rate (given in units of radians per second, radians per second, g units, and radians per second, respectively). The effectors are aileron, rudder, asymmetric stabilator, yaw thrust vectoring, and roll thrust vectoring (all given in units of degrees).

Finite differencing was used to generate the Jacobians. Table A1 contains the perturbation step size on states and effectors used to generate the Jacobians. These Jacobians are listed in table A2.

Table A1. Finite Differencing Perturbation Sizes

State	Perturbation size	Effector	Perturbation size, deg
ν_s	$V_T/10$ ft/sec	δ_{ail}	2
p_s	.08 rad/sec	δ_{rud}	↓
r_s	.08 rad/sec	δ_{as}	↓
ϕ_s	.04 rad	δ_{ytv}	↓
		δ_{rtv}	↓

The open-loop roll and spiral mode poles for each flight condition are shown in figure A1. Figure A2 shows the open-loop Dutch roll frequency and damping. Figure A3 contains plots of the two open-loop eigenvector characteristics used in the numerical examples to quantify modal coupling. Note that the ϕ-to-β ratio is nondimensional.

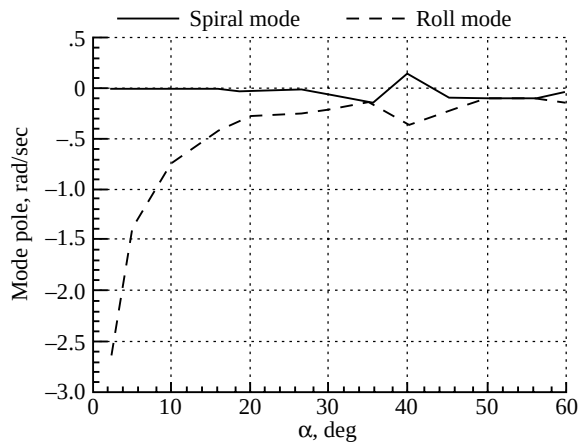

Figure A1. Roll and spiral mode poles of open-loop aircraft.

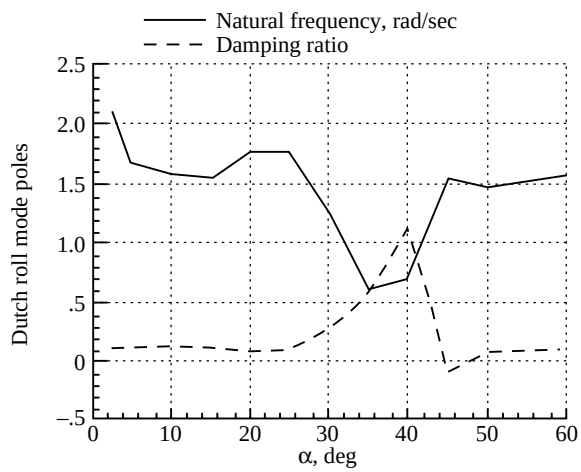

Figure A2. Dutch roll mode pole of open-loop aircraft.

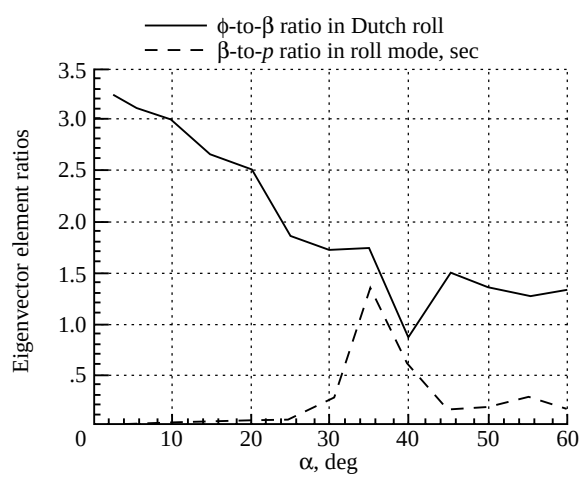

Figure A3. ϕ-to-β in Dutch roll and β-to-p roll mode eigenvector element ratios of open-loop aircraft.

Table A2. HARV Jacobians

$\alpha = 2.5^\circ \qquad V_T = 837$ ft/sec

A =

−0.1855	0.0072	−836.1471	32.1675
−0.0271	−2.7580	0.6086	0.0000
0.0058	0.1084	−0.1614	0.0000
0.0000	1.0000	0.0000	0.0000

B =

−0.0946	0.5304	−0.2000	0.2628	0.0056
0.4398	0.0578	0.4538	−0.0048	0.0181
−0.0209	−0.0419	−0.0171	−0.0317	−0.0015
0.0000	0.0000	0.0000	0.0000	0.0000

M =

0.0000	0.9990	−0.0436	0.0000
0.0000	0.0436	0.9990	0.0000
−0.0030	0.0964	−0.0560	0.0000
−0.0002	0.0000	−0.9993	0.0384

N =

0.0000	0.0000	0.0000	0.0000	0.0000
0.0000	0.0000	0.0000	0.0000	0.0000
−0.0197	−0.0009	−0.0218	−0.0041	−0.0008
−0.0001	0.0006	−0.0002	0.0003	0.0000

$\alpha = 5^\circ \qquad V_T = 598$ ft/sec

A =

−0.1305	0.1512	−597.5921	32.1675
−0.0187	−1.5272	0.6757	0.0000
0.0050	0.1152	−0.1529	0.0000
0.0000	1.0000	0.0000	0.0000

B =

−0.0551	0.2975	−0.1025	0.2461	0.0024
0.2746	0.0314	0.2224	−0.0059	0.0176
−0.0283	−0.0242	−0.0161	−0.0294	−0.0019
0.0000	0.0000	0.0000	0.0000	0.0000

M =

0.0000	0.9962	−0.0872	0.0000
0.0000	0.0872	0.9962	0.0000
−0.0021	0.0535	−0.0462	0.0000
−0.0002	0.0003	−0.9992	0.0538

Table A2. Continued

N =

0.0000	0.0000	0.0000	0.0000	0.0000
0.0000	0.0000	0.0000	0.0000	0.0000
−0.0134	−0.0002	−0.0100	−0.0038	−0.0007
−0.0001	0.0005	−0.0002	0.0004	0.0000

$\alpha = 10^\circ$ $V_T = 421$ ft/sec

A =

−0.0955	0.1610	−420.2861	32.1674
−0.0194	−0.8687	0.6852	0.0000
0.0062	0.1333	−0.1871	0.0000
0.0000	1.0000	0.0000	0.0000

B =

−0.0286	0.1409	−0.0358	0.2500	0.0006
0.1350	0.0146	0.1010	−0.0085	0.0177
−0.0261	−0.0130	−0.0161	−0.0291	−0.0032
0.0000	0.0000	0.0000	0.0000	0.0000

M =

0.0000	0.9848	−0.1736	0.0000
0.0000	0.1736	0.9848	0.0000
−0.0012	0.0295	−0.0392	0.0000
−0.0002	0.0004	−0.9991	0.0765

N =

0.0000	0.0000	0.0000	0.0000	0.0000
0.0000	0.0000	0.0000	0.0000	0.0000
−0.0068	−0.0002	−0.0042	−0.0038	−0.0007
−0.0001	0.0003	−0.0001	0.0006	0.0000

$\alpha = 15^\circ$ $V_T = 361$ ft/sec

A =

−0.0702	0.1331	−360.9948	32.1679
−0.0185	−0.5227	0.6580	0.0000
0.0069	0.1218	−0.2358	0.0000
0.0000	1.0000	0.0000	0.0000

B =

−0.0198	0.0873	−0.0149	0.2497	−0.0013
0.0817	0.0078	0.0618	−0.0105	0.0174
−0.0236	−0.0089	−0.0160	−0.0282	−0.0045
0.0000	0.0000	0.0000	0.0000	0.0000

Table A2. Continued

M =

0.0000	0.9659	−0.2588	0.0000
0.0000	0.2588	0.9659	0.0000
−0.0007	0.0169	−0.0407	0.0000
−0.0002	0.0004	−0.9994	0.0891

N =

0.0000	0.0000	0.0000	0.0000	0.0000
0.0000	0.0000	0.0000	0.0000	0.0000
−0.0044	−0.0002	−0.0026	−0.0037	−0.0006
−0.0001	0.0002	0.0000	0.0007	0.0000

$\alpha = 20°$ $V_T = 334$ ft/sec

A =

−0.0558	0.0399	−333.9384	32.1655
−0.0236	−0.2994	0.6024	0.0000
0.0095	0.0932	−0.2796	0.0000
0.0000	1.0000	0.0000	0.0000

B =

−0.0076	0.0559	−0.0079	0.2406	0.0038
0.0463	0.0037	0.0451	−0.0121	0.0160
−0.0183	−0.0061	−0.0168	−0.0262	−0.0063
0.0000	0.0000	0.0000	0.0000	0.0000

M =

0.0000	0.9397	−0.3420	0.0000
0.0000	0.3420	0.9397	0.0000
−0.0005	0.0069	−0.0477	0.0000
−0.0002	0.0001	−1.0002	0.0963

N =

0.0000	0.0000	0.0000	0.0000	0.0000
0.0000	0.0000	0.0000	0.0000	0.0000
−0.0026	−0.0002	−0.0021	−0.0036	−0.0007
0.0000	0.0002	0.0000	0.0007	0.0000

$\alpha = 25°$ $V_T = 307$ ft/sec

A =

−0.0472	−0.0569	−308.1857	32.1649
−0.0191	−0.2336	0.5856	0.0000
0.0103	0.0901	−0.3405	0.0000
0.0000	1.0000	0.0000	0.0000

Table A2. Continued

B =

0.0108	0.0375	0.0061	0.2548	0.0027
0.0315	0.0005	0.0355	−0.0158	0.0169
−0.0162	−0.0035	−0.0180	−0.0260	−0.0084
0.0000	0.0000	0.0000	0.0000	0.0000

M =

0.0000	0.9063	−0.4226	0.0000
0.0000	0.4226	0.9063	0.0000
−0.0002	0.0007	−0.0544	0.0000
−0.0002	−0.0002	−1.0006	0.1044

N =

0.0000	0.0000	0.0000	0.0000	0.0000
0.0000	0.0000	0.0000	0.0000	0.0000
−0.0015	−0.0001	−0.0018	−0.0037	−0.0008
0.0000	0.0001	0.0000	0.0008	0.0000

$\alpha = 30^{\circ}$ $\quad V_T = 282$ ft/sec

A =

−0.0403	−0.1336	−282.2590	32.1549
−0.0099	−0.3858	0.7811	0.0000
0.0060	0.2001	−0.5262	0.0000
0.0000	1.0000	−0.0280	0.0000

B =

0.0195	0.0270	0.0183	0.2471	0.0007
0.0211	−0.0006	0.0288	−0.0167	0.0166
−0.0137	−0.0022	−0.0185	−0.0243	−0.0099
0.0000	0.0000	0.0000	0.0000	0.0000

M =

0.0000	0.8660	−0.5000	0.0000
0.0000	0.5000	0.8660	0.0000
−0.0007	0.0041	−0.0675	0.0000
−0.0001	−0.0005	−1.0009	0.1140

N =

0.0000	0.0000	0.0000	0.0000	0.0000
0.0000	0.0000	0.0000	0.0000	0.0000
−0.0008	0.0000	−0.0013	−0.0036	−0.0008
0.0001	0.0001	0.0001	0.0009	0.0000

Table A2. Continued

$\alpha = 35^\circ \qquad V_T = 268$ ft/sec

A =

−0.0423	−0.2074	−267.5458	31.9377
−0.0027	−0.3022	0.8106	0.0000
0.0019	0.1766	−0.6487	0.0000
0.0000	1.0000	−0.1202	0.0000

B =

0.0246	0.0214	0.0250	0.2432	0.0007
0.0155	−0.0011	0.0246	−0.0183	0.0155
−0.0124	−0.0015	−0.0196	−0.0226	−0.0112
0.0000	0.0000	0.0000	0.0000	0.0000

M =

0.0000	0.8192	−0.5736	0.0000
0.0000	0.5736	0.8192	0.0000
−0.0012	−0.0048	−0.0715	0.0000
−0.0002	−0.0008	−1.0010	0.1195

N =

0.0000	0.0000	0.0000	0.0000	0.0000
0.0000	0.0000	0.0000	0.0000	0.0000
−0.0005	−0.0001	−0.0011	−0.0036	−0.0008
0.0001	0.0001	0.0001	0.0009	0.0000

$\alpha = 40^\circ \qquad V_T = 261$ ft/sec

A =

−0.0435	−0.2705	−261.6818	31.4210
0.0003	−0.3069	0.6522	0.0000
−0.0018	0.2127	−0.6251	0.0000
0.0000	1.0000	−0.2193	0.0000

B =

0.0257	0.0181	0.0277	0.2401	0.0007
0.0125	−0.0018	0.0210	−0.0198	0.0143
−0.0123	−0.0008	−0.0208	−0.0208	−0.0124
0.0000	0.0000	0.0000	0.0000	0.0000

M =

0.0000	0.7660	−0.6428	0.0000
0.0000	0.6428	0.7660	0.0000
−0.0018	−0.0081	−0.0628	0.0000
−0.0002	−0.0010	−1.0008	0.1202

Table A2. Continued

N =

0.0000	0.0000	0.0000	0.0000	0.0000
0.0000	0.0000	0.0000	0.0000	0.0000
−0.0004	−0.0001	−0.0011	−0.0036	−0.0008
0.0001	0.0001	0.0001	0.0009	0.0000

$\alpha = 45^\circ$ $V_T = 262$ ft/sec

A =

−0.0383	−0.2061	−261.3775	30.5801
−0.0105	0.1843	0.0830	0.0000
0.0088	−0.2481	−0.1543	0.0000
0.0000	1.0000	−0.3264	0.0000

B =

0.0079	0.0162	0.0265	0.2349	0.0007
0.0109	−0.0030	0.0247	−0.0211	0.0131
−0.0129	0.0004	−0.0269	−0.0189	−0.0135
0.0000	0.0000	0.0000	0.0000	0.0000

M =

0.0000	0.7071	−0.7071	0.0000
0.0000	0.7071	0.7071	0.0000
−0.0012	−0.0350	−0.0210	0.0000
−0.0001	−0.0008	−0.9994	0.1169

N =

0.0000	0.0000	0.0000	0.0000	0.0000
0.0000	0.0000	0.0000	0.0000	0.0000
−0.0009	−0.0001	−0.0011	−0.0036	−0.0008
0.0000	0.0001	0.0001	0.0009	0.0000

$\alpha = 50^\circ$ $V_T = 262$ ft/sec

A =

−0.0333	0.0412	−261.3253	29.4804
−0.0077	−0.0330	0.2272	0.0000
0.0084	−0.0162	−0.3423	0.0000
0.0000	1.0000	−0.4366	0.0000

B =

−0.0118	0.0147	0.0367	0.2294	0.0007
0.0087	−0.0035	0.0240	−0.0222	0.0117
−0.0129	0.0014	−0.0290	−0.0170	−0.0144
0.0000	0.0000	0.0000	0.0000	0.0000

Table A2. Continued

M =

0.0000	0.6428	−0.7660	0.0000
0.0000	0.7660	0.6428	0.0000
−0.0008	−0.0122	−0.0208	0.0000
−0.0001	0.0002	−0.9985	0.1126

N =

0.0000	0.0000	0.0000	0.0000	0.0000
0.0000	0.0000	0.0000	0.0000	0.0000
−0.0016	−0.0001	−0.0003	−0.0036	−0.0008
0.0000	0.0001	0.0001	0.0009	0.0000

$\alpha = 55^\circ$ $V_T = 266$ ft/sec

A =

−0.0380	0.1644	−265.4073	28.4186
−0.0065	−0.0508	0.2138	0.0000
0.0087	0.0197	−0.3784	0.0000
0.0000	1.0000	−0.5303	0.0000

B =

−0.0145	0.0143	0.0719	0.2260	0.0007
0.0064	−0.0030	0.0309	−0.0229	0.0103
−0.0124	0.0011	−0.0380	−0.0150	−0.0152
0.0000	0.0000	0.0000	0.0000	0.0000

M =

0.0000	0.5736	−0.8192	0.0000
0.0000	0.8192	0.5736	0.0000
−0.0009	−0.0050	−0.0240	0.0000
−0.0001	0.0006	−0.9990	0.1070

N =

0.0000	0.0000	0.0000	0.0000	0.0000
0.0000	0.0000	0.0000	0.0000	0.0000
−0.0017	−0.0002	0.0018	−0.0036	−0.0008
−0.0001	0.0001	0.0003	0.0009	0.0000

$\alpha = 60^\circ$ $V_T = 276$ ft/sec

A =

−0.0472	0.1523	−275.5784	26.6075
−0.0058	−0.0638	0.2364	0.0000
0.0089	0.0320	−0.3957	0.0000
0.0000	1.0000	−0.6794	0.0000

Table A2. Concluded

$\mathbf{B} =$

−0.0156	0.0144	0.1012	0.2251	−0.0071
0.0051	−0.0022	0.0227	−0.0236	0.0107
−0.0131	−0.0001	−0.0296	−0.0128	−0.0144
0.0000	0.0000	0.0000	0.0000	0.0000

$\mathbf{M} =$

0.0000	0.5000	−0.8660	0.0000
0.0000	0.8660	0.5000	0.0000
−0.0013	−0.0083	−0.0097	0.0000
−0.0002	0.0006	−0.9995	0.0965

$\mathbf{N} =$

0.0000	0.0000	0.0000	0.0000	0.0000
0.0000	0.0000	0.0000	0.0000	0.0000
−0.0018	−0.0003	0.0037	−0.0034	−0.0001
−0.0001	0.0001	0.0004	0.0008	0.0000

Appendix B

Baseline HARV Flight Control System Gains

This appendix contains the linear feed-forward and measurement feedback gains for the 13 flight conditions considered. There are two controls and five effectors. As previously stated, the effectors are aileron, rudder, asymmetric stabilator, yaw thrust vectoring, and roll thrust vectoring (which are all measured in degrees). The measurements are body-axis roll and yaw rate (which are measured in radians per second), sensed lateral acceleration (which is measured in g units), and sensed sideslip rate (which is measured in radians per second). The controls are commanded roll and yaw acceleration (which are measured in radians per second squared). The feed-forward and measurement feedback gain matrices are listed in table B1.

The feed-forward gains are designed such that the two controls are mapped into the five effectors. The two controls are commanded roll and yaw angular acceleration. The feed-forward gain matrix is a Jacobian of a control mapping algorithm (discussed in ref. 6), which is evaluated at the various trimmed flight conditions. For the purposes of this research, the set of feed-forward gain matrices is assumed to be given. The controls are a sum of pilot input and feedback (fig. 3),

$$\mathbf{u} = \mathbf{K}(\mathbf{u}_{FB} + \mathbf{u}_{\text{pilot}})$$

The measurement feedback gain matrices map the four measurements into the two controls such that

$$\mathbf{u}_{FB} = \mathbf{G}\mathbf{z}$$

The baseline gains listed were designed using the CRAFT (control power, robustness, agility, and flying-qualities trade-offs) procedure of reference 2. These gains are designed to be scheduled with angle of attack.

Table B1. Feed-Forward and Feedback Gain Matrices

$\alpha = 2.5^\circ$

$\mathbf{K} =$

2.4595	1.6767
−1.5926	−34.1549
0.3513	2.5021
0.0000	0.0000
0.0000	0.0000

$\mathbf{G} =$

−0.1062	−0.6541	0.0441	−0.2824
−0.0642	0.1223	0.0460	2.1799

$\alpha = 5^\circ$

$\mathbf{K} =$

4.0206	2.4478
−5.6765	−62.0159
0.8725	4.9350
0.0000	0.0000
0.0000	0.0000

$\mathbf{G} =$

−0.5442	−0.7925	−0.0019	−0.3825
−0.0625	0.1133	0.0524	1.7372

$\alpha = 10^\circ$

$\mathbf{K} =$

6.9486	2.5159
−21.1127	−116.4603
2.3793	8.9879
0.0000	0.0000
0.0000	0.0000

$\mathbf{G} =$

−1.1081	−1.2024	−0.1014	−0.1852
−0.0437	0.1778	0.0607	1.7539

$\alpha = 15^\circ$

$\mathbf{K} =$

10.1457	−0.9134
−27.6594	−103.2218
3.4755	7.2567
−6.1403	−21.9256
0.0000	0.0000

Table B1. Continued

$\mathbf{G} =$

−1.2663	−1.1728	−0.0005	−0.6436
0.0228	0.2459	0.0600	1.5931

$\alpha = 20°$

$\mathbf{K} =$

14.2474	−5.3125
−33.5753	−90.8832
5.0302	3.8308
−11.3867	−30.2217
0.0000	0.0000

$\mathbf{G} =$

−1.4859	−2.0383	−0.6063	−1.2320
0.0681	0.3996	0.2004	1.9451

$\alpha = 25°$

$\mathbf{K} =$

14.1097	−14.4480
−41.1839	−84.1229
4.7607	−1.7777
−13.5142	−28.1494
0.0000	0.0000

$\mathbf{G} =$

−1.5959	−1.9635	0.3622	−1.1257
0.0885	0.4970	0.0183	2.1152

$\alpha = 30°$

$\mathbf{K} =$

13.2511	−23.2949
−47.7514	−75.2633
3.9250	−7.5768
−15.1551	−25.5799
0.0000	0.0000

$\mathbf{G} =$

−0.4186	−2.2548	0.1121	−1.2376
−0.2107	0.7058	−0.0254	1.6765

Table B1. Continued

$\alpha = 35°$

$\mathbf{K} =$

11.7391	−33.3489
−58.3414	−70.4668
1.8687	−14.4658
−17.7790	−24.7922
0.0000	0.0000

$\mathbf{G} =$

0.1880	−2.2674	−0.2291	−0.9062
−0.3412	0.7287	−1.3296	1.3411

$\alpha = 40°$

$\mathbf{K} =$

13.9902	−46.6544
−70.6014	−56.1793
0.3247	−18.6618
−19.3750	−22.5693
0.0000	0.0000

$\mathbf{G} =$

0.1116	−1.7216	0.0175	−0.4289
−0.3338	0.3032	−2.8258	1.2669

$\alpha = 45°$

$\mathbf{K} =$

10.6672	−61.5933
−83.7570	−38.0300
−6.8896	−16.0345
−20.8578	−20.3934
7.3404	−8.0219

$\mathbf{G} =$

−0.4819	−0.8720	−0.6353	−1.0400
0.1811	0.3329	−0.2938	1.5237

$\alpha = 50°$

$\mathbf{K} =$

−11.8843	−76.7698
−92.7368	−22.1658
−11.4007	−12.8837
−22.4435	−18.4057
10.6763	−13.8889

Table B1. Concluded

$\mathbf{G} =$

−0.1495	−1.0156	−0.2759	−0.9231
−0.0301	0.4716	0.2016	1.3646

$\alpha = 55^\circ$

$\mathbf{K} =$

−29.1475	−83.0683
−89.7036	−0.6993
−2.1824	−1.6032
−25.2961	−17.2914
11.6376	−18.5082

$\mathbf{G} =$

−0.1753	−0.8326	−0.0765	−0.7941
−0.0716	0.4357	0.1557	1.5059

$\alpha = 60^\circ$

$\mathbf{K} =$

−37.1976	−83.9399
−66.6277	0.3374
0.0000	0.0000
−27.7290	−15.5958
13.9318	−27.0141

$\mathbf{G} =$

−0.4204	−0.5479	−0.3657	−0.1400
0.0113	0.3407	0.2077	1.3010

References

1. Pahle, Joseph W.; Powers, Bruce; Regenie, Victoria; Chacon, Vince; DeGroote, Steve; and Murnyak, Steven: *Research Flight-Control System Development for the F-18 High Alpha Research Vehicle.* NASA TM-104232, 1991.

2. Murphy, Patrick C.; and Davidson, John B.: Control Design for Future Agile Fighters. AIAA-91-2882, Aug. 1991.

3. Andry, A. N., Jr.; Shapiro, E. Y.; and Chung, J. C.: Eigenstructure Assignment for Linear Systems. *IEEE Trans. Aerosp. & Electron. Syst.*, vol. AES-19, no. 5, Sept. 1983, pp. 711–729.

4. Davidson, J. B.; and Schmidt, D. K.: *Flight Control Synthesis for Flexible Aircraft Using Eigenspace Assignment.* NASA CR-178164, 1986.

5. McRuer, Duane; Ashkenas, Irving; and Graham, Dunstan: *Aircraft Dynamics and Automatic Control.* Princeton Univ. Press, 1973.

6. Lallman, Frederick J.: *Relative Control Effectiveness Technique With Application to Airplane Control Coordination.* NASA TP-2416, 1985.

7. Buttrill, Carey S.; Arbuckle, P. Douglas; and Hoffler, Keith D.: *Simulation Model of a Twin-Tail, High Performance Airplane.* NASA TM-107601, 1992.

8. Burden, Richard L.; and Faires, J. Douglas: *Numerical Analysis, 4th ed.* PWS-KENT Publ. Co., 1989.

References

1. Pahle, Joseph W.; Powers, Bruce; Regenie, Victoria; Chacon, Vince; DeGroote, Steve; and Murnyak, Steven: *Research Flight-Control System Development for the F-18 High Alpha Research Vehicle.* NASA TM-104232, 1991.

2. Murphy, Patrick C.; and Davidson, John B.: Control Design for Future Agile Fighters. AIAA 91-2882, Aug. 1991.

3. Andry, A. N., Jr.; Shapiro, E. Y.; and Chung, J. C.: Eigenstructure Assignment for Linear Systems. *IEEE Trans. Aerosp. & Electron. Syst.*, vol. AES-19, no. 5, Sept. 1983, pp. 711–729.

4. Davidson, J. B.; and Schmidt, D. K.: *Flight Control Synthesis for Flexible Aircraft Using Eigenspace Assignment.* NASA CR-178164, 1986.

5. McRuer, Duane; Ashkenas, Irving; and Graham, Dunstan: *Aircraft Dynamics and Automatic Control.* Princeton Univ. Press, 1973.

6. Lallman, Frederick J.: *Relative Control Effectiveness Technique With Application to Airplane Control Coordination.* NASA TP-2416, 1985.

7. Buttrill, Carey S.; Arbuckle, P. Douglas; and Hoffler, Keith D.: *Simulation Model of a Twin-Tail, High Performance Airplane.* NASA TM-107601, 1992.

8. Burden, Richard L.; and Faires, J. Douglas: *Numerical Analysis, 4th ed.* PWS-KENT Publ. Co., c.1989.

REPORT DOCUMENTATION PAGE

Form Approved
OMB No. 0704-0188

Public reporting burden for this collection of information is estimated to average 1 hour per response, including the time for reviewing instructions, searching existing data sources, gathering and maintaining the data needed, and completing and reviewing the collection of information. Send comments regarding this burden estimate or any other aspect of this collection of information, including suggestions for reducing this burden, to Washington Headquarters Services, Directorate for Information Operations and Reports, 1215 Jefferson Davis Highway, Suite 1204, Arlington, VA 22202-4302, and to the Office of Management and Budget, Paperwork Reduction Project (0704-0188), Washington, DC 20503.

1. AGENCY USE ONLY *(Leave blank)*

2. REPORT DATE
June 1994

3. REPORT TYPE AND DATES COVERED
Technical Memorandum

4. TITLE AND SUBTITLE
Predicting the Effects of Unmodeled Dynamics on an Aircraft Flight Control System Design Using Eigenspace Assignment

5. FUNDING NUMBERS
WU 505-64-52-01

6. AUTHOR(S)
Eric N. Johnson, John B. Davidson, and Patrick C. Murphy

7. PERFORMING ORGANIZATION NAME(S) AND ADDRESS(ES)
NASA Langley Research Center
Hampton, VA 23681-0001

8. PERFORMING ORGANIZATION REPORT NUMBER
L-17333

9. SPONSORING/MONITORING AGENCY NAME(S) AND ADDRESS(ES)
National Aeronautics and Space Administration
Washington, DC 20546-0001

10. SPONSORING/MONITORING AGENCY REPORT NUMBER
NASA TM-4548

11. SUPPLEMENTARY NOTES
Johnson: The George Washington University, Washington, D.C.; Davidson and Murphy: Langley Research Center, Hampton, VA.

12a. DISTRIBUTION/AVAILABILITY STATEMENT
Unclassified–Unlimited

Subject Category 08

12b. DISTRIBUTION CODE

13. ABSTRACT *(Maximum 200 words)*
When using eigenspace assignment to design an aircraft flight control system, one must first develop a model of the plant. Certain questions arise when creating this model as to which dynamics of the plant need to be included in the model and which dynamics can be left out or approximated. The answers to these questions are important because a poor choice can lead to closed-loop dynamics that are unpredicted by the design model. To alleviate this problem, a method has been developed for predicting the effect of not including certain dynamics in the design model on the final closed-loop eigenspace. This development provides insight as to which characteristics of unmodeled dynamics will ultimately affect the closed-loop rigid-body dynamics. What results from this insight is a guide for eigenstructure control law designers to aid them in determining which dynamics need or do not need to be included and a new way to include these dynamics in the flight control system design model to achieve a required accuracy in the closed-loop rigid-body dynamics. The method is illustrated for a lateral-directional flight control system design using eigenspace assignment for the NASA High Alpha Research Vehicle (HARV).

14. SUBJECT TERMS
Eigenspace assignment; Unmodeled dynamics; High Alpha Research Vehicle; Lateral-directional aircraft control system

15. NUMBER OF PAGES
39

16. PRICE CODE
A03

17. SECURITY CLASSIFICATION OF REPORT
Unclassified

18. SECURITY CLASSIFICATION OF THIS PAGE
Unclassified

19. SECURITY CLASSIFICATION OF ABSTRACT

20. LIMITATION OF ABSTRACT